AFRL-AFOSR-UK-TR-2010-0012

Nonlinear Structuring and High-energy Electrons: Role in Ionosphere and in Thunderstorm Atmosphere Processes

Aleksander Viktorovich Gurevich

P. N. Lebedev Physical Institute
Leninsky pr.,53
Moscow, Russia 117924

EOARD ISTC 06-7004

May 2010

Final Report for 01 February 2007 to 01 February 2010

Air Force Research Laboratory
Air Force Office of Scientific Research
European Office of Aerospace Research and Development
Unit 4515 Box 14, APO AE 09421

REPORT DOCUMENTATION PAGE

Form Approved OMB No. 0704-0188

1. REPORT DATE *(DD-MM-YYYY)*	2. REPORT TYPE	3. DATES COVERED *(From – To)*
12-05-2010	Final Report	01-Feb-07 - 01-Feb-10

4. TITLE AND SUBTITLE

Nonlinear Structuring and High-energy Electrons: Role in Ionosphere and in Thunderstorm Atmosphere Processes

5a. CONTRACT NUMBER
ISTC Registration No: 3641p

5b. GRANT NUMBER
ISTC 06-7004

5c. PROGRAM ELEMENT NUMBER
61102F

6. AUTHOR(S)

Dr. Aleksander Viktorovich Gurevich

5d. PROJECT NUMBER

5d. TASK NUMBER

5e. WORK UNIT NUMBER

7. PERFORMING ORGANIZATION NAME(S) AND ADDRESS(ES)

P. N. Lebedev Physical Institute
Leninsky pr.,53
Moscow 117924
Russia

8. PERFORMING ORGANIZATION REPORT NUMBER

ISTC 06-7004

9. SPONSORING/MONITORING AGENCY NAME(S) AND ADDRESS(ES)

EOARD
Unit 4515 BOX 14
APO AE 09421

10. SPONSOR/MONITOR'S ACRONYM(S)
AFRL/AFOSR/EOARD

11. SPONSOR/MONITOR'S REPORT NUMBER(S

AFRL-AFOSR-UK-TR-2010-0012

12. DISTRIBUTION/AVAILABILITY STATEMENT

Approved for public release; distribution is unlimited.

13. SUPPLEMENTARY NOTES

14. ABSTRACT

This report results from a contract tasking P. N. Lebedev Physical Institute as follows: The Project includes five Tasks:

1. The modification of the magnetosphere by the controllable flow of fast electrons coming upwards from the artificially modified ionosphere. Theoretical investigation and the conception of the experimental program.
2. The formation of super-narrow ionosphere structures in ionosphere artificially modified by powerful radio waves in double-resonance conditions. The super-narrow structures serve for the strong scattering of UHF radio waves. Theoretical investigation and the conception of the experimental program.
3. The generation of powerful gamma emission, powerful bipolar radio pulses and optic emission from the high-altitude thunder discharges. Theoretical investigation, comparison with the existing observations and plans of future experiments.
4. High-energy particles in thunder phenomena. Experimental and theoretical investigation of intensive gamma emission, generation of HF and VHF radio waves, electric field, electric field variations.
5. Transformation of an extensive atmospheric shower in the thunder electric field: intensive growth of electromagnetic component, namely of the high-energy electrons number, of gamma quanta and positrons number. Space enlargement of the shower. Experimental and theoretical investigation.

Expected results:

1. The theory of the effects arising in the magnetosphere modified by the controllable flux of fast electrons coming upwards from the artificially modified ionosphere. The evaluation of the possibilities to observe these effects.

2. The evaluation of the possibility to form the elongated super-narrow structures in the ionosphere artificially modified by powerful radio waves in double-resonance conditions. The evaluation of the UHF radio wave scattering off these structures.
3. The theory of the high-altitude thunder discharges generating of the powerful gamma emission, powerful bipolar pulses of radio emission and the optic emission.
4. The theory of the runaway breakdown for the case of very high values of electric field observed in the lightning stepped leader which led to the effective generation of high-energy particles and intensive fluxes of gamma emission.
5. The results of detailed simultaneous measurements of the set of parameters associated with the lightning. In particular, the value of the electric field and it's variations, the radio emission in HF and VHF diapasons, the gamma emission. All measurements will be realized from several registration points.
6. The results of simultaneous measurements of the set of parameters associated with the extensive atmosphere shower (EAS) passing through the thundercloud. In particular, the characteristics of high-energy electrons, muons and gamma emission, the radio emission in HF and VHF diapasons and the value of the electric field and it's variations. All measurements will be realized from several registration points.
7. The theoretical interpretation of the measurements associated with the EAS passing through the thundercloud.

1. The theory of the ultra low-frequency MHD ionosphere waves generation was developed. These waves could be generated by the action on ionosphere by modulated microwaves. The exciting currents serving as a source of Alfven and magnetoacoustic waves were estimated. The power of the radiated waves and the effective coefficient of radiation were calculated as a function of the modulation frequency.
2. The theory of the generation of the super narrow striations aligned along the Earth magnetic field was developed. These structures can arise in ionosphere under the action of powerful radio wave having frequency close to both upper hybrid frequency and to a multiple gyromagnetic frequency. The developed theory was compared to the results of HAARP experiments.
3. The theory of the high altitude atmosphere discharge arising under the combined action of the runaway breakdown in a thunderstorm electric field and the passing of an extensive atmosphere shower was developed.
4. The theory of runaway breakdown (RB) for the case of a strong electric field was developed. The dependence of the fast electron distribution function and their number on the electric field value was calculated. The numerical simulation of electron generation was done taking into account space non-uniformity of the electric field.
5. The investigation of the correlation between cosmic rays and the bursts of radio and gamma emissions was carried out at the Tien-Shan Mountain Cosmic Ray Station. Both electric field and its variation were registered as well. The data analysis discovered cases of short-time bursts having the complex composition: electrons accelerated up to about 10 – 30 MeV, gamma quanta of low (tens keV) and high (hundred keV) energies. The time correlation between short bursts of emission with the lightning discharges registered by the electromagnetic trigger was established. The space correlation of these bursts with the presence of electrically charged clouds nearby the the experimental facility. The composite energy spectrum of short gamma bursts was measured.
6. The short time bursts of electron flow amplified by thunderstorm electric field were registered directly. They are observed exclusively during the active phase of a thunderstorm, absolutely being absent during fine weather, rain (even heavy) or a snowfall. In some cases the correlation of accelerated electrons bursts with the moment of the extensive atmosphere showers (EAS) passing was observed. The events of such kind could be treated as the direct observation of the lightning discharge generation by the EAS particles.
7. The event of the gamma background fall correlated in time with the thunderstorm discharge. This event could be treated as the first direct observation of the earlier predicted form of the discharge (RB-EAS discharge). This type of discharge occurs in thunderstorm atmosphere when EAS passes through the thunderstorm electric field.

15. SUBJECT TERMS
EOARD, Atmospheric Sciences, Atmospheric Physics, Ionosphere structuring, radio wave scattering, plasma waves, runaway breakdown, thunderstorm, atmosphere discharges

16. SECURITY CLASSIFICATION OF:			17. LIMITATION OF ABSTRACT	18, NUMBER OF PAGES	19a. NAME OF RESPONSIBLE PERSON
a. REPORT	b. ABSTRACT	c. THIS PAGE			SCOTT DUDLEY, Lt Col, USAF
UNCLAS	UNCLAS	UNCLAS	SAR	65	19b. TELEPHONE NUMBER *(Include area code)* +44 (0)1895 616162

ISTC Project No. 3641p

Nonlinear structuring and high-energy electrons: role in ionosphere and in thunderstorm atmosphere processes

Final Project Technical Report

on the work performed from February 1, 2008 to January 31, 2010

P. N. Lebedev Physical Institute of the Russian Academy of Sciences (RAS)

Project Manager — A.V. Gurevich, academician, Doctor of Science

Director — M.A. Vasiliev, Doctor of Science

March 2010

This work was supported financially by EOARD and performed under the agreement with the International Science and Technology Center (ISTC), Moscow.

Title of the Project:	Nonlinear structuring and high-energy electrons: role in ionosphere and in thunderstorm atmosphere processes
Commencement Date:	02.01.09
Duration:	36 months
Project Manager	Aleksandr Viktorovich Gurevich
phone number:	+7(499)1236414
fax number:	+7(499)1357880
e-mail address:	alex@lpi.ru
Leading Institute:	P. N. Lebedev Physical Institute of the Russian Academy of Sciences (RAS) Leninskii pr. 53, Moscow Russia, 119991 +7(499)1352430 postmaster@sci.lebedev.ru www.lebedev.ru

Keywords: Ionosphere structuring, radio wave scattering, plasma waves, runaway breakdown, thunderstorm, atmosphere discharges

March 2010

This work was supported financially by EOARD and performed under the agreement with the International Science and Technology Center (ISTC), Moscow.

LIST OF THE CONTENST

This work was supported financially by EOARD and performed under the agreement with the International Science and Technology Center (ISTC), Moscow.

Brief description of the work plan

The Project includes five Tasks:

1. The modification of the magnetosphere by the controllable flow of fast electrons coming upwards from the artificially modified ionosphere. Theoretical investigation and the conception of the experimental program.
2. The formation of super-narrow ionosphere structures in ionosphere artificially modified by powerful radio waves in double-resonance conditions. The super-narrow structures serve for the strong scattering of UHF radio waves. Theoretical investigation and the conception of the experimental program.
3. The generation of powerful gamma emission, powerful bipolar radio pulses and optic emission from the high-altitude thunder discharges. Theoretical investigation, comparison with the existing observations and plans of future experiments.
4. High-energy particles in thunder phenomena. Experimental and theoretical investigation of intensive gamma emission, generation of HF and VHF radio waves, electric field, electric field variations.
5. Transformation of an extensive atmospheric shower in the thunder electric field: intensive growth of electromagnetic component, namely of the high-energy electrons number, of gamma quanta and positrons number. Space enlargement of the shower. Experimental and theoretical investigation.

Expected results:

1. The theory of the effects arising in the magnetosphere modified by the controllable flux of fast electrons coming upwards from the artificially modified ionosphere. The evaluation of the possibilities to observe these effects.
2. The evaluation of the possibility to form the elongated super-narrow structures in the ionosphere artificially modified by powerful radio waves in double-resonance conditions. The evaluation of the UHF radio wave scattering off these structures.
3. The theory of the high-altitude thunder discharges generating of the powerful gamma emission, powerful bipolar pulses of radio emission and the optic emission.
4. The theory of the runaway breakdown for the case of very high values of electric field observed in the lightning stepped leader which led to the effective generation of high-energy particles and intensive fluxes of gamma emission.
5. The results of detailed simultaneous measurements of the set of parameters associated with the lightning. In particular, the value of the electric field and it's variations, the radio emission in HF and VHF diapasons, the gamma emission. All measurements will be realized from several registration points.
6. The results of simultaneous measurements of the set of parameters associated with the extensive atmosphere shower (EAS) passing through the thundercloud. In particular, the characteristics of high-energy electrons, muons and gamma emission, the radio emission in HF and VHF diapasons and the value of the electric field and it's variations. All measurements will be realized from several registration points.
7. The theoretical interpretation of the measurements associated with the EAS passing through the thundercloud.

Technical Approach and Methodology

Tasks 1-3

The theoretical approach to these Tasks is based on:

1. Method of the nonlinear Boltzman kinetic equation.
2. Nonlinear kinetic theory of plasma.

3. Analytical analysis of the nonlinear equations using expansion over small parameters.
4. Numerical simulations.

Tasks 4 and 5

1. Modification of the NaI scintillate system. Decrease of the digitations time interval of the signal registration up to 1 μs. Extension of the system.
2. Modification of the registration system for "slow" and "fast" components of the electric field in order to registry them with 10 –100 ns accuracy.
3. Extension of the VHF registration systems and expansion of VHF receiver bandwidth up to 1-3 MHz.
5. Expansion of the Geiger-Muller registration system up to effective area 1 km^2.
6. Creation of the hadron - muon detector with effective area up to 0.5 km^2 for the fixation of EAS coming.
7. Calibration of all detectors, in particular, using standard Cs137 sources.
8. Investigation of the effect of the thunder electric field on the registration system in order to minimize the noise and to discard the false signals.
9. Registration of EAS, gamma and radio emission in thunder conditions and investigation of their interconnection.
10. Investigation of the interconnection of EAS with lightning generation.

Results

Task 1: Modification of the magnetosphere by the controllable flow of fast electrons coming upwards from the artificially modified ionosphere. Theoretical investigation and the conception of the experimental program

The small-scale perturbations of ionosphere plasma arising under the action of the high-frequency powerful radio wave are one of the most significant phenomena discovered in the modification experiments. These perturbations are the plasma density depletion. A large number of of physical effects, from anomalous radio wave absorption up to SEE, are connected with these perturbations. An ensemble of such perturbations creates the average plasma density depletion aligned along the magnetic field. The investigation of the effects connected with such regions of plasma density decreasing are considered in the Project. Point is that balance of the system is provided by the currents flowing along the boundaries of the regions. If the amplitude of the pump wave is modulated with some frequency the modulation of the plasma heating and, correspondingly, the oscillating current arise in turn. These currents can lead to the generation of MHD waves of ultra low frequency.

A theoretical investigation of the excitation of MHD plasma waves in Earth magnetosphere under the action of high-frequency powerful radio waves was considered. The high-frequency wave is supposed to be modulated by a low frequency signal. As it is known the powerful radio wave form striations several kilometers long in the ionosphere plasma, were the electron temperature increases for 2-4 times [1]. The heat spreads from the resonance layer along the magnetic field. If the radio wave is modulated with a low frequency the electric currents are excited near the resonance layer. These currents could serve as sources of MHD waves.

We assume that the magnetic field is directed along the vertical axis *z*. The area of the radio wave acting has radius R (*R* is about 10 km). We neglect the heat transfer across the magnetic field and the recombination losses. The resonance layer is assumed to be thin. In these assumptions the heat transfer equation has the form:

$$\frac{\partial}{\partial z}(\kappa_{\parallel}\frac{\partial \tau}{\partial z}) - b(\tau - 1) + \delta(z)(\alpha + \beta\cos\Omega t) = \frac{\partial \tau}{\partial t} \qquad (1)$$

Here $\tau = T/T_\infty$, were T_∞ – the temperature out of the heating region. The longitudinal thermal-conductivity coefficient $\kappa_{\parallel}$ depends on the temperature as $\kappa_{\parallel} = a\tau^{5/2}$ [2], the second term describes the energy losses in collisions of electrons with neutral molecules and ions, $b = \delta\nu$, were ν – the effective collision rate, δ - the energy fraction lost in the collision (it is about m_e/m_i). Third term describes the action of the radio wave, Ω – the modulation frequency (it is about 1 Hz).

Note, that due to plasma quasi-neutrality both electrons and ions take part in the diffusion (ambipolar diffusion). At the same time electrons play the main role in the energy transfer. That's way the temperature perturbations are much higher that the density ones, which we have neglected here.

1) *Stationary temperature perturbation*

Let us treat non-stationary temperature perturbation as a small one:

$$\tau(z) = \tau_0(z) + \Delta\tau(z,t), \quad |\Delta\tau| \ll \tau \qquad (2)$$

To solve the equation a new variable is defined

$$y = \tau^{7/2}, \quad y(z) = y_0(z) + \Delta y(z,t) \qquad (3)$$

It leads to the equation for y_0

$$-\frac{2}{7}ay_0'' + b(y_0^{2/7} - 1) = \alpha\delta(z) \qquad (4)$$

Using natural boundary condition $y_0' \to 0$ at $y_0 \to 1$ the solution of (4) should be obtained

$$y_0' = -sgn(z)\sqrt{7\frac{a}{b}\left(\frac{7}{9}y_0^{9/7} - y_0 + \frac{2}{9}\right)} \qquad (5)$$

At large distances the perturbation decrease exponentially with the characteristic scale $l = \sqrt{a/b}$

The condition at zero should be also taken into account:

$$\frac{7}{9}Y_0^{9/7} - Y_0 + \frac{2}{9} = \frac{7\alpha^2}{16ab}, \quad Y_0 = y_0(0) \qquad (6)$$

2) Non-stationary temperature perturbation

Equation for Δy has the form

$$\frac{\partial \Delta y}{\partial t} - ay_0^{5/7}\frac{\partial^2 \Delta y}{\partial z^2} + b\Delta y = \frac{7}{2}Y_0^{5/7}\beta\delta(z)\cos\Omega t \qquad (7)$$

Let the solution form to be $\Delta y = Re[f(z)e^{i\Omega t}]$

We obtain

$$f'' - \frac{\kappa^2}{y_0^{5/7}} f = 0, \quad z \neq 0, \quad \kappa^2 = \frac{b + i\Omega}{a} \tag{8}$$

$$f(+0) - f(-0) = -\frac{7\beta}{2a} \tag{9}$$

Obviously, the asymptotic behavior of the solution is:

$$f(z) \sim e^{-\kappa|z|}, \quad z \to \infty, \quad Re\,\kappa > 0 \tag{10}$$

The solution of the equation in WKB approximation:

$$f = C y_0^{5/28} e^{-\kappa F(|z|)}, \quad F(z) = \int_0^z \frac{d\eta}{y_0^{5/14}(\eta)} \tag{11}$$

The usability condition of the WKB approximation in the case is: $|\kappa|l>>1$, in another words $\Omega>>b$ (12)

(Collision frequency in the ionosphere F-layer ν is about 100 Hz, δ is about

$(30\cdot1836)^{-1}=2\cdot10^{-5}$, thus . $\delta\nu \sim 10^{-3}$ Гц . $\ll \Omega$).

Constant. C is determined from the matching condition at $z=0$:

$$\Delta f'(0) = C\left(\frac{5}{28} Y_0^{-23/28} \Delta y_0'(0) - 2\kappa Y_0^{-5/28}\right) = -\frac{7B}{2a} \tag{13}$$

$$C = \frac{7\beta Y_0^{5/28}}{\frac{5}{4}\alpha Y_0^{-9/14} + 4a\kappa} = |C| e^{i\varphi} \tag{14}$$

Thus, the solution for Δy has the form:

$$\Delta y(z,t) = |C| y_0^{5/28} e^{-\kappa_1 F(|z|)} \cos[\Omega t + \varphi - \kappa_2 F(|z|)], \quad \kappa = \kappa_1 + i\kappa_2 \tag{15}$$

Finally, returning to , we obtain for the temperature:

$$\Delta\tau(z,t) = \frac{2}{7} y_0^{-5/7} \Delta y = \frac{2}{7} |C| y_0^{-15/28} e^{-\kappa_1 F(|z|)} \cos[\Omega t + \varphi - \kappa_2 F(|z|)] \tag{16}$$

The characteristic scale of this distribution is $L = 1/|\kappa| \sim \sqrt{a/\Omega} \sim 10$ km.

In reality temperature does not decrease so strong out of the heating area. There is some boundary layer. Its width could be estimated using the fraction of longitudinal and transverse heating transfer $\kappa_\parallel/\kappa_\perp = (\omega_e/\nu)^2$, were . ω_e - the electron cyclotron frequency. For boundary layer width

, we have $\kappa_\parallel/L^2 \sim \kappa_\perp/h^2$. So, $h \sim L/(\omega_e\tau_e)$. In our case $\omega_e \sim 10^7$ Hz, thus in the case $h \sim$ 1 m.

Thus we have estimated the temperature oscillations induced by the absorption of the pump mode in the Earth ionosphere. Now the problem of the oscillating currents should be considered. They are the sources of magneto-hydrodynamic waves.

The equation of continuity and the equation of the motion in the frame of the two two-fluid hydrodynamics model have the form [2]:

$$\frac{\partial n_e}{\partial t} + \mathrm{div}(n_e\vec{v}_e) = 0 \quad (17)$$

$$\frac{\partial n_i}{\partial t} + \mathrm{div}(n_i\vec{v}_i) = 0 \quad (18)$$

$$m_e n_e(\frac{\partial \vec{v}_e}{\partial t} + (\vec{v}_e\nabla)\vec{v}_e) = -\nabla p_e - en_e(\vec{E} + \frac{1}{c}[\vec{v}_e, \vec{B}]) + \vec{R} \quad (19)$$

$$m_i n_i(\frac{\partial \vec{v}_i}{\partial t} + (\vec{v}_i\nabla)\vec{v}_i) = -\nabla p_i + en_i(\vec{E} + \frac{1}{c}[\vec{v}_i, \vec{B}]) - \vec{R} \quad (20)$$

Here we have neglected the viscosity and assume $Z = 1$.

- the interaction force between electrons and ions, composed of the friction force and the thermal force.

Note, the Debye radius is about one centimeter in ionosphere plasma, while the characteristic dimension of the system under consideration is about one kilometer. Thus the quasi-neutrality approximation is well fulfilled $n_e = n_i \equiv n$.

Let us turn to linear combinations of the obtained equations taking into account the relations $n_e = n_i$ and $m_e \ll m_i$.

Equation for hydrodynamic velocity $\vec{V} = (m_e\vec{v}_e + m_i\vec{v}_i)/(m_e + m_i) \simeq \vec{v}_i$ (the sum of equations (19) and (20)):

$$\rho\frac{d\vec{V}}{dt} = -\nabla p + \frac{1}{c}[\vec{j}\vec{B}] \quad (21)$$

(here $\rho = m_i n$, $p = p_e + p_i$, $\vec{j} = en(\vec{v}_i - \vec{v}_e)$).

Generalized Ohm law (the difference of equations (19) and (20), previously divided on the corresponding masses):

$$\vec{E} + \frac{1}{c}[\vec{V}\vec{B}] + \frac{1}{en_e}(\nabla p_e - \vec{R}_T) = \frac{\vec{j}_\parallel}{\sigma_\parallel} + \frac{\vec{j}_\perp}{\sigma_\perp} + \frac{1}{en_e c}[\vec{j}\vec{B}] \quad (22)$$

here $\sigma_\perp = e^2 n\tau_e/m_e$ ($\tau_e = \nu^{-1}$), $\sigma_\parallel = 2\sigma_\perp$; thermal force for the case of strongly magnetized plasma: $\vec{R}_T = -0.71n\nabla_\parallel T$.

The electric field is potential $\vec{E} = -\nabla\varphi$ and the term containing gradient of the pressure leads to the renormalization of the potential only, it can be omitted.

Note, that here and further on fields $\vec{E}$, velocities $\vec{V}$, and currents $\vec{j}$ represent the fluctuating parts of the total quantities (i.e. changing proportionally to $e^{i\Omega t}$). Just the

fluctuating parts will produce MHD waves in the final analysis). The term $(\vec{V}\nabla)\vec{V}$ should be neglected in the linear approximation.

Finally, subtracting (18) from (17) and taking into account the quasi-neutrality criterion, the current closure condition could be obtained:

$$\operatorname{div} \vec{j} = 0. \tag{23}$$

The electric field is determined from this condition in the case of quasi-neutral plasma [3]. Longitudinal and the transverse components of the electric field (relative to magnetic field) are:

$$\vec{E}_{\|} + 0.7\frac{\nabla_{\|} T_e}{e} = \frac{\vec{j}_{\|}}{\sigma_{\|}} \tag{24}$$

$$\vec{E}_{\perp} + \frac{1}{c}[\vec{V}\vec{B}] = \frac{\vec{j}_{\perp}}{\sigma_{\perp}} + \frac{1}{enc}[\vec{j}_{\perp}\vec{B}]. \tag{25}$$

Multiplying (21) over and using $\vec{V} \sim e^{i\Omega t}$, one obtain $\vec{B}$

$$[\vec{V}\vec{B}] = \frac{iB^2}{\Omega\rho c}\vec{j}_{\perp} \tag{26}$$

It is seen from the equation (21), the pressure has an shock at the heating region boundary. It leads to the origin of diamagnetic current $\vec{j}_{\varphi}$ circulating along the cylinder boundary in the layer with the thickness h:

$$\vec{j}_{\varphi} = -\frac{nc}{B^2}[\nabla T_e \vec{B}] = -\frac{nc}{B} T_0 \Delta\tau(z,t)\delta(r-R)\vec{e}_{\varphi} \tag{27}$$

Turning back to the Ohm law and substituting (26) into (25) we obtain:

$$\vec{E}_{\perp} + \mathcal{R}\vec{j}_{\perp} = \vec{j}_{\perp}/\sigma_{\perp} + \frac{1}{enc}[\vec{j}_{\perp}\vec{B}] \tag{28}$$

Here $\mathcal{R} = \frac{iB^2}{\Omega\rho c^2}$.

The comparing $\mathcal{R}, \sigma^{-1}$ and B/enc give:

$$\mathcal{R}\sigma \sim \frac{m_e}{m_i}\frac{\omega_e^2}{\Omega\nu} \sim 10^6$$

$$\mathcal{R}\frac{enc}{B} \sim \frac{m_e}{m_i}\frac{\omega_e}{\Omega} \sim 100$$

So, the main role belongs to the resistance $\mathcal{R}$. Due to the potentiality and axial symmetry of the electric field $E_{\varphi} = 0$. Thus the bulk current φ is small: $j_{\varphi} < j_r$

The system of equations is:

$$E_z + \frac{0.7}{e}\frac{\partial T}{\partial z} = \frac{j_z}{\sigma} \tag{29}$$

$$E_r = \mathcal{R} j_r \tag{30}$$

Here $\sigma \equiv \sigma_{||}$

The equation for the potential should be obtained using $\vec{E} = -\nabla\varphi$ and the closure condition (23):

$$\frac{\partial}{\partial z}\left(\sigma\frac{\partial\varphi}{\partial z}\right) + \frac{1}{\mathcal{R}}\frac{1}{r}\left(r\frac{\partial\varphi}{\partial r}\right) = \frac{0.7}{e}\frac{\partial}{\partial z}\left(\sigma\frac{\partial T}{\partial z}\right) \tag{31}$$

Inside the heating region $\varphi \simeq 0.7T/e$.
Outside the heating region we have the equation:

$$\frac{\partial}{\partial z}\left(\sigma\frac{\partial\varphi}{\partial z}\right)+\frac{1}{\mathcal{R}}\frac{1}{r}\left(r\frac{\partial\varphi}{\partial r}\right), \tag{32}$$

where $\sigma = const$.
The coordinate transform $r' = \sqrt{\mathcal{R}\sigma}r$ reduces the problem to:

$$\triangle'\varphi = -4\pi\varrho(z), \tag{33}$$

where $\varrho = -\frac{0.7}{4\pi e}\frac{\partial^2 T}{\partial z^2}$, at that the source has the form of a flat "pancake" with the thickness L and the radius $\sqrt{\mathcal{R}\sigma}R$.

Let us make use of electrostatic analogy — the problem of plane capacitor electric field. We are interested in the electric field behavior at its border, exactly there the transverse component does arise, and thus the current flows. It is seen that if we do the inverse transformation, that currents flow in the thin boundary layer with thickness $L/\sqrt{\mathcal{R}\sigma}$ only.

Let us consider the auxiliary problem. Let the charge plane $(-R < x < 0, -\infty < y < +\infty)$, were R is very large, have the plane charge density ψ. The component of the electric field E_x in the point with coordinates (X,Y,Z), $X>0$ should obtained.

We have:

$$E_x = \int\int \frac{\psi\,(-x+X)\,dx\,dy}{((-x+X)^2+(-y+Y)^2+(-z+Z)^2)^{3/2}} = 2\psi\int_0^R \frac{(x+X)\,dx}{(x+X)^2+(Z-z)^2} =$$

$$= \psi\,\ln\left(\frac{R^2}{X^2+(z-Z)^2}\right)$$

For the neutral is average layer with the finite thickness and charge density ϱ,the electric field is:

$$E_x = -\int \varrho(z)\ln(X^2+(z-Z)^2)\,dz \tag{34}$$

For our problem, taking into account that during the back transformation electric field is transformed as $\partial\varphi/\partial r = \sqrt{\mathcal{R}\sigma}\partial\varphi/\partial r'$ the current j_r has the form:

$$j_r(r,z) = \frac{0.7}{4\pi e}\sqrt{\sigma/\mathcal{R}}\int\frac{\partial^2 T}{\partial z'^2}\ln(\mathcal{R}\sigma\Delta r^2+(z'-z)^2)dz', \tag{35}$$

where $\Delta r = r - R$.

Thus, the structure of the currents being the sources of electromagnetic waves was investigated. Now let us consider the problem of MHD wave emission.

General theory

Let us consider the system of magnetic hydrodynamic equations

$$\frac{\partial\rho}{\partial t}+\mathrm{div}(\rho\vec{v})=0, \quad \frac{ds}{dt}=0 \tag{36}$$

$$\rho\frac{d\vec{v}}{dt} = -\nabla p + \frac{1}{4\pi}[\mathrm{rot}\,\vec{H},\vec{H}] \tag{37}$$

$$\frac{\partial\vec{H}}{\partial t} = \mathrm{rot}[\vec{v},\vec{H}], \quad \mathrm{div}\,\vec{H} = 0 \tag{38}$$

The external current which is the source of the waves should be singled out of the total current:

$$\mathrm{rot}\,\vec{H} = \frac{4\pi}{c}(\vec{j}^{\,i} + \vec{j}^{\,e}) \tag{39}$$

Here *i* and *e* mark the internal and external currents.

Only the ponderomotive force should be included in the equation. It affects on the internal current, what corresponds to the transformation in the equation:

$$\mathrm{rot}\vec{H} \rightarrow \mathrm{rot}\vec{H} - \frac{4\pi}{c}\vec{j}^{\,e} \tag{40}$$

The linearized equations could be obtained by considering the magnetic field and the density exiting $\vec{h}$ and ρ' to be small and neglecting the quadratic in velocity term $(\vec{v}\nabla)\vec{v}$:

$$\frac{\partial\vec{h}}{\partial t} = \mathrm{rot}[\vec{v},\vec{H}], \quad \mathrm{div}\,\vec{h} = 0 \tag{41}$$

$$\frac{\partial\rho'}{\partial t} + \rho\,\mathrm{div}\,\vec{v} = 0 \tag{42}$$

$$\rho\frac{d\vec{v}}{dt} = -u_0^2\nabla\rho' + \frac{1}{4\pi}[\mathrm{rot}\,\vec{h},\vec{H}] - \frac{1}{c}[\vec{j}^{\,e},\vec{H}] \tag{43}$$

In the case the sound velocity $u_0 = \sqrt{(\partial p/\partial\rho')_s} \sim 10^4 - 10^5$ cm/s is much less then the Al'fven velocity $V_A = H/\sqrt{4\pi\rho} \sim 10^8$ cm/s. Thus the term containing the density gradient should be neglected as well.

The equation on $\vec{v}$ could be obtained by differentiating (43) and using (41):

$$\rho\frac{\partial^2\vec{v}}{\partial t^2} = \frac{1}{4\pi}[\mathrm{rot}\ \mathrm{rot}[\vec{v},\vec{H}],\vec{H}] + \frac{1}{c}\left[\vec{H},\frac{\partial\vec{j}^{\,e}}{\partial t}\right] \tag{44}$$

It is convenient to rewrite (44) in cylindrical coordinates, where it decay in two equations:

$$\frac{\partial^2 v_r}{\partial t^2} = V_A^2\left(\frac{\partial^2 v_r}{\partial z^2} + \frac{\partial^2 v_r}{\partial r^2} + \frac{1}{r}\frac{\partial v_r}{\partial r} - \frac{1}{r^2}v_r\right) - \frac{H}{\rho c}\frac{\partial j_\varphi}{\partial t} \tag{45}$$

$$\frac{\partial^2 v_\varphi}{\partial t^2} = V_A^2\frac{\partial^2 v_\varphi}{\partial z^2} + \frac{H}{\rho c}\frac{\partial j_r}{\partial t} \tag{46}$$

The wave vector k does not have the φ component due to the symmetry. Thus it is seen that equation (31) describes the medium oscillations in the $k - H$ plane. It corresponds to the fast magnetic sonic wave. The equation (32) describes the oscillations perpendicular to the $k - H$ plane. It corresponds to the Alfven's wave.

Alfven's wave

To solve the equation (46) with the current determined by (35) the Green function should by found as the solution of the equation:

$$\frac{\partial^2 g}{\partial t^2} - V_A^2 \frac{\partial^2 g}{\partial z^2} = \delta(z) e^{i\Omega t} \tag{47}$$

Taking into account that the required wave is outgoing one, it should be obtained that:

$$g = \frac{e^{i\Omega t - ik|z|}}{2ikV_A^2}, \tag{48}$$

where $k = \Omega / V_A$.

The solution in the point $Z > 0, Z >> L$.

$$v_\varphi = e^{i\Omega t - ikZ} \frac{H}{2\rho c V_A} \int j_r(z) e^{ikz} dz \tag{49}$$

Note, that $V_A/\Omega \sim 1000$ км $\gg L$. Thus the exponent should be expanded. Taking into account $\varrho \sim \partial^2 T / \partial z^2$ we obtain

$$\int j_r(z)\, dz = j_r(z) z\, dz = 0, \tag{50}$$

and thus the first nonzero term will contain z^2.

The wave propagates in the thin boundary layer and thus $v_\varphi = V\delta(r - R)$. Then the right part of the equation should be integrated over the thickness. As a result omitting the factor exp $(i\Omega t - ikz)$ we obtain:

$$V = -\frac{0.7}{8\pi} \frac{H}{\rho c e} \frac{k^2}{V_A^2} \sqrt{\frac{\sigma}{\mathcal{R}}} \int\int\int \frac{\partial^2 T}{\partial z'^2} z^2 \ln(\mathcal{R}\sigma \Delta r^2 + (z' - z)^2) dz'\, dr\, dz \tag{51}$$

To estimate the integral we suppose $\Delta\tau \simeq \Delta\tau(0) e^{-|z|/L}$ and use the characteristic measurements $z \sim z' \sim L$, $\Delta r \sim L/\sqrt{\mathcal{R}\sigma}$. Then the velocity should be estimated accurate within the numerical factor:

$$V \sim \frac{H}{\rho c e} \frac{\Omega^2}{V_A^4} \frac{\Delta T_0 L^3}{\mathcal{R}} \sim \frac{\Delta T_0}{eHL} \left(\frac{\Omega L}{V_A}\right)^3 \frac{c}{V_A} L \tag{52}$$

Magnetic sonic wave

Let us consider the equation (45). Let $v_r = v$. The nonuniformity should be taken into account by integrating the equation in the vicinity of the point $r = R$.

$$\frac{\partial^2 v}{\partial t^2} = V_A^2 \left(\frac{\partial^2 v_r}{\partial z^2} + \frac{\partial^2 v}{\partial r^2} + \frac{1}{r}\frac{\partial v}{\partial r} - \frac{1}{r^2} v \right), \quad r \neq R \tag{53}$$

$$\frac{\partial v}{\partial r}|_{R+0} - \frac{\partial v}{\partial r}|_{R-0} = \frac{4\pi n T_0}{H^2} \frac{\partial \Delta\tau}{\partial t} \tag{54}$$

The Fourier transform over z and t of these equations should be done so that:

$$v = \int\int u(\omega, k_z, r) e^{ik_z z - i\omega t} dk_z d\omega \tag{55}$$

$$\Delta\tau = \int\int \widetilde{\Delta\tau}(\omega, k_z) e^{ik_z z - i\omega t} dk_z d\omega \tag{56}$$

.

Equations take the form:

$$-\omega^2 u = V_A^2 \left[-k_z^2 u + \frac{\partial^2 u}{\partial r^2} + \frac{1}{r}\frac{\partial u}{\partial r} - \frac{u}{r^2} \right] \tag{57}$$

$$\frac{\partial u}{\partial r}|_{R+0} - \frac{\partial u}{\partial r}|_{R-0} = -\frac{4\pi n T_0}{H^2} i\omega \widetilde{\Delta\tau} \equiv U(\omega, k_z) \tag{58}$$

Marking $\alpha^2 = \omega^2/V_A^2 - k_z^2$ and substituting $x = \alpha r$ the equation we reduce (57) to the Bessel equation of the first order:

$$\frac{\partial^2 u}{\partial x^2} + \frac{1}{x}\frac{\partial u}{\partial x} + (1 - \frac{1}{x^2})u = 0 \tag{59}$$

The solution of (57) has the form

$$u = \begin{cases} E(\omega, k_z) J_1(\alpha r), & r < R \\ B(\omega, k_z) J_1(\alpha r) + D(\omega, k_z) Y_1(\alpha r), & r > R \end{cases} \tag{60}$$

Substituting this solution into (58) we obtain:

$$\begin{cases} E J_1(\alpha R) = B J_1(\alpha R) + D Y_1(\alpha R) \\ E J_1'(\alpha R) + U/\alpha = B J_1'(\alpha R) + D Y_1'(\alpha R) \end{cases} \tag{61}$$

These are two equations on three unknown quantities and we have to apply an additional restriction on coefficients E, D and α. It should depend on the sign of α^2.

1) $\alpha^2 > 0 \Leftrightarrow k_z^2 > \omega^2/V_A^2$

The solution at $r > R$ must give the outgoing wave. Quantity can be taken in the form U.

$$U = a(k_z)\delta(\omega - \Omega) + a^*(k_z)\delta(\omega - \Omega) \tag{62}$$

Then the solution should be $u \sim H_1^{(1)}\delta(\omega - \Omega) + H_1^{(2)}\delta(\omega + \Omega)$

Coefficients E, D are also taken in the form $D = D_-\delta(\omega - \Omega) + D_+\delta(\omega - \Omega)$, and then the additional condition could be obtained:

$$D_- = iE_-; \quad D_+ = -iE_+ \tag{63}$$

Solving the obtained set of equations and using the expression for Wronskian $J_1'(x)Y_1(x) - J_1(x)Y_1'(x) = -2/(\pi x)$ we obtain the solution:

$$u(\omega, k_z, r) = \begin{cases} -i\frac{\pi}{2} R a(k_z) H_1^{(1)}(\alpha R) J_1(\alpha r)\delta(\omega - \Omega) + \text{к. с.} \cdot \delta(\omega + \Omega), & r < R \\ -i\frac{\pi}{2} R a(k_z) H_1^{(1)}(\alpha r) J_1(\alpha R)\delta(\omega - \Omega) + \text{к. с.} \cdot \delta(\omega + \Omega), & r > R \end{cases} \tag{64}$$

(к.с. - complex conjugation)

2) $\alpha^2 < 0 \Leftrightarrow k_z^2 > \omega^2/V_A^2$

Let $\beta^2 = -\alpha^2$.

The solution finite in infinity expressed over the modified Bessel function has the form:

$$u(\omega, k_z, r) = \begin{cases} G(\omega, k_z) I_1(\beta r), & r < R \\ Q(\omega, k_z) K_1(\beta r), & r > R \end{cases} \tag{65}$$

Substituting it into (58) we obtain the set

$$\begin{cases} G I_1(\beta R) = Q K_1(\beta R) \\ G I_1'(\beta R) + U/\beta = Q K_1'(\beta R) \end{cases} \tag{66}$$

Finding the coefficients and using the expression for Wronskian $I_1(x)K_1'(x) - I_1'(x)K_1(x) = -1/x$, we obtain finally:

$$u(\omega, k_z, r) = \begin{cases} -Ra(k_z) K_1(\beta R) I_1(\beta r) \delta(\omega - \Omega) + \text{к. с.} \cdot \delta(\omega + \Omega), & r < R \\ -Ra(k_z) K_1(\beta r) I_1(\beta R) \delta(\omega - \Omega) + \text{к. с.} \cdot \delta(\omega + \Omega), & r > R \end{cases} \tag{67}$$

We found the asymptotic expression for the wave at large $\varkappa$, when $r = R$ for simplicity. According to (55), (64), (67):

$$v(t, z, R) = 2e^{-i\Omega t} \left[-i\frac{\pi}{2} R \int_0^{\Omega/V_A} a(k_z) H_1^{(1)}(\alpha R) J_1(\alpha R) \cos(k_z z)\, dk_z - \right.$$

$$\left. - R \int_{\Omega/V_A}^{+\infty} a(k_z) K_1(\beta R) I_1(\beta R) \cos(k_z z)\, dk_z \right] + \text{к.с.}$$

The characteristic value of the argument $a(k_z)$ is $1/L$. Taking into account that $L \sim R \ll V_A/\Omega$ and $\beta \simeq |k_z|$ we can suppose that the integrand changes just a little within the range $[0, V_A/\Omega]$ we obtain $(x = k_z R,\ \eta = z/R)$

$$v(t, z, R) = 2e^{-i\Omega t} \int_0^{\infty} a(x/R) K_1(x) I_1(x) \cos(x\eta) dx + \text{к.с.} \tag{68}$$

It is well known that the convolution of the product of two functions is equal to the Fourier transform of these functions. The Fourier transform of $a(k_z)$ was calculated earlier (see (62) and (58)), and for $K_1 I_1$ we use the known formula:

$$\int_0^{\infty} K_1(x) I_1(x) \cos(xy) dx = \frac{\pi}{4} \frac{F(\frac{3}{2}; \frac{3}{2}; 3; -\frac{4}{y^2})}{|y|^3} \tag{69}$$

Obviously $F(\frac{3}{2}; \frac{3}{2}; 3; -\frac{4}{y^2}) \to 1, \quad y \to \infty$.

The function $\Delta\tau(\eta)$ is concentrated mainly in the region $|\eta| < L/R \sim 1$. When $\eta \gg 1$ we have

$$\int_0^\infty a(x/R)K_1(x)I_1(x)\cos(x\eta)dx \sim \int_{-\infty}^{+\infty} \frac{F(\frac{3}{2};\frac{3}{2};3;-\frac{4}{y^2})}{|y|^3}\Delta\tau(\eta-y)dy \simeq$$

$$\simeq \int_{-\infty}^{+\infty} \frac{\Delta\tau(\eta-y)}{y^3}dy = \int_{-\infty}^{+\infty} \frac{\Delta\tau(y)}{(\eta-y)^3}dy \simeq \frac{1}{\eta^3}\int \Delta\tau(y)dy$$

It is seen that at large z $v(t,r,z) \sim 1/z^3$.

Resume

1) The temperature disturbances of the ionosphere arise under the action of the powerful radio wave modulated with low frequency $\Omega \sim 1$ – 100 Hz. They propagate as waves decaying on the length about $L \sim 10$ km.

2) Two types of currents appear in these structures: the diamagnetic current circulating along the circle near the tube boundary and the current flowing in the boundary layer in the vertical direction. The last starts at the middle and returns on the tube buts. The current of the first type excites the magnetic sonic wave, while of the second type – the Alfven wave. At that the Alfven wave is channeled inside the tube while the magnetic sonic wave propagates in all directions. That why the Alfen wave have the possibility to propagate on distances larger then the magnetic sonic wave in spite of the fact that its amplitude is small due to the smallness of transversal conductivity and due to the quadrupole character of the emission.

3) The analysis of the obtained results show also that the energy fraction transferred into Alfen wave strongly depends on the modulation frequency increasing with its growth. On the contrary, the amplitude of the magneto-sonic wave practically do not depend on the modulation frequency.

References

1. Gurevich A.V., Lukyanov A.V., Zybin K.P. Phys. Lett. A, **206** 247 (1995)
2. Gurevich A.V. Physics Uspekhi, **177** (11) 1145-1177 (2007)
3. Leontovich M.A. (ed.) Reviews of plasma physics, vol.3 (Moscow, 1963)
4. Chen F. Introduction to plasma physics and control fusion, Springer, 2006.

Task 2.: Formation of super-narrow ionosphere structures in ionosphere artificially modified by powerful radio waves in double-resonance conditions. The super-narrow structures serve for the strong scattering of UHF radio waves. Theoretical investigation and the conception of the experimental program.

Theory

Theory of the formation of super-narrow structures aligned along magnetic field was developed. These inhomogeneities arise in ionosphere under the action of powerful pump radio wave when its frequency is close both to the upper-hybrid frequency and to the multiple electron gyro frequency. Upper-hybrid waves excited in these conditions are trapped in the regions of local plasma density depletions. Moreover, low-range Bernstein modes are generated as a result of the decay processes. Bernstein modes being phase-correlated with stationary upper-hybrid waves are also stationary. Stationary Bernstein waves produce plasma

inhomogeneiteis aligned along magnetic field. According to the theory these ingomogeneities can scatter radio waves having frequences up to 1 – 3 GHz.

The striations appear due to resonance excitation of upper hybrid (UH) waves by the powerful pump radio wave in the vicinity of upper hybrid resonance point Z_{uh} in the ionosphere determined by relation:

$$\omega_{pe}^2(Z_{UH}) = \omega_0^2 - \Omega_e^2 \qquad (1)$$

Here $\omega 0$ is the pump wave frequency, ω_{pe} is the Langmuir plasma frequency ($\omega^2_{pe} = 4\pi e^2 N_e(z)/m$) and Ω_e is electron gyrofrequency ($\Omega_e = eH/mc$).

Let us discuss now the special conditions when UH resonance point Z^d_{uh} is close to the multiple gyroresonance $n\Omega_e$:

$$\omega_0 \approx n\Omega_e, \qquad \omega_{pe}^2(Z^d_{UH}) = \Omega_e^2(n^2 - 1), \qquad n = 3,4,5,6,..... \qquad (2)$$

Thus in the vicinity of Z^d_{UH} double resonance conditions are fulfilled:

$$\omega_0 \approx \omega_{pe} \approx n\Omega_e .$$

In the vicinity of Z^d_{uh} the pattern of striation is changed strongly. First of all according to nonlinear theory [1] in resonance region the number density of striations is strongly diminishing with approaching of relative pump frequency shift $\Delta\omega = \omega_0 - n\Omega_e$ to the resonance point. Exactly at resonance $\Delta\omega = 0$ striations disappeared, but their number is growing rapidly at small shifts $\Delta\omega = (0.005–0.01)\omega_0$ to the both sides from resonance. Together with striations at double resonance point disappear the anomalous absorption both pump and probe waves propagating in the resonance region. Naturally, quite analogous behavior demonstrates the field aligned scattering (FAS) determined by striations. The experimental observations near multiple gyroresonance region (MGR) agree well with the theory [2,3].

In MGR region stimulated electromagnetic emission (SEE) is strongly changed as well. In the downshifted region $\Delta\omega < 0$ only downshifted (DM) structures and its long tail in SEE is seen. In the resonance point $\Delta\omega = 0$ DM structure disappears fully. In the upshifted region both DM structure and a new one broad upshifted maximum (BUM) structures are seen. The behavior of SEE emission in MGR
region have the theoretical explanation. The existence of BUM feature in upshifted region is connected with the excitation of Bernstein waves.

The dispersion equation of these waves according to the theory [4-5] has a form:

$$1 - \frac{\omega_{pe}^2}{\omega_0^2 - \Omega_e^2} - \frac{m\omega_{pe}^2}{\omega_0^2 - n^2\Omega_e^2} K_{n-1}(k^2\rho^2) = 0 \qquad (3)$$

Here Ω_e is gyrofrequency, ρ is electron Larmour radius, k is perpendicular wave vector and $K_n(x) \approx xn/(2nn!)$, $x<<1$ is modified Bessel function.

In [6] it was shown, that Bernstein waves with $k_{||} >> k$ can be excited above upper hybrid resonance layer by second order four-wave interaction process. An important aspect of the BUM is that the frequency of excited wave is higher than the frequency of the pump wave. It means that the simple three-wave decay process cannot be responsible for this effect. That is why the four wave interaction was supposed already in the first quantitative explanations [7]. The detailed theory was developed by Huang and Kuo [8]. This process involved two pump wave “photons”, upper hybrid plasmon, an electron Bernstein plasmon and driving low frequency oscillation near the low hybrid wave frequency. The second harmonic oscillation ($2\omega_0$, $k_0 \approx 0$) associated with the HF heater wave acts as the pump of the process. The frequency upshifted upper hybrid wave (ω_2, k_2) and the frequency downshifted electron Bernstein wave (ω_1, k_1) are the sideband and the decay mode of the decay process, respectively. A low frequency electrostatic oscillations (ω_s, k) in the frequency range of low hybrid waves $\omega_{lh} = (\omega_{pe}\Omega_e)^{1/2}$ is also induced by nonlinear coupling with HF waves. Resonance conditions

$$\omega_1 + \omega_s^* = \omega_0 = \omega_2 - \omega_s, \qquad (2\omega_1 = \omega_s^* + \omega_2), \qquad k_1 + k = 0 = k_2 - k \tag{4}$$

are supposed to be fulfilled.

This process is considered to be the main mechanism for generation of the BUM features observed in stimulated electromagnetic emission. The threshold of the pump electric field for this parametric process has a form [8]:

$$E_{th} = \frac{m}{c}\frac{\omega_0(\omega_0+\Omega_e)}{k}\left|\frac{\omega_s^2-\omega_{lh}^2}{\omega_{lh}^2}\right|^{1/2}\frac{\Omega_e}{\omega_{uh}}\left[\frac{2\nu_e^2(1+\Omega_e^2)/\omega_{uh}\omega_{eb}\omega_2\left(\omega_{eb}^2-\omega_2^2\right)^2}{(\omega_{eb}^2-\Omega_e^2)(\omega_2^2-\Omega_e^2)(n^2\Omega_2^2-\omega_{eb}^2)(\omega_2^2-n^2\Omega_e^2)}\right]^{1/4} \tag{5}$$

Here ω_{eb} is electron Bernstein frequency.

For typical ionospheric conditions in the vicinity of 4th gyroresonance $f_0 - 4f_c$ = 5–60 kHz and for $f_2 \approx f_{\mathrm{BUM}}$ = 20–80 kHz the threshold field E_{th} = 0.2–0.6 V/m, the corresponding instability increment $\gamma \approx$ 500–100 s^{-1}. It means that elongated perturbations ($k_{\parallel} << k$) associated with electron Bernstein could be really excited in ionospheric modification experiments.

Let us emphasize now a very important new feature of the effect. Bernstein waves are excited in four-wave interaction process. This process is considered in the theory as interaction of free waves propagating in homogeneous plasma [2]. But in real ionosphere conditions situation is different. The upper hybrid waves which play significant role in four-wave process are not free. They are excited due to resonance instability, trapped inside striations and cannot exist outside them in resonance region [1]. It means that the upper hybrid waves exist as *standing* waves inside striations only. A wave moving to the right direction has a strong phase correlation with a wave moving to the left.

This *attribute* of upper hybrid waves affect strongly the four-wave process. First—Bernstein waves could be excited inside striations only, where UH waves exist. Second, the decay conditions (4) for upper hybrid wave moving to the right and to the left direction are identical. It means that the Bernstein waves excited in decaying process of two pump wave "photon" into upper hybrid plasmon and Bernstein plasmon are standing wave as well. The excitation of standing Bernstein waves is very important because this standing wave can serve as a source of new quasi-stable small scale density perturbations. Actually, due to the action of striction force the standing waves can generate small-scale elongated magnetic field density disturbances. To calculate this effect let us consider kinetic equation for electrons moving in external magnetic field and in standing Bernstein wave $E = E_{eb}\sin(k_{eb}x)\cos(\omega_{eb}t)$:

$$\frac{\partial f}{\partial t} + \mathbf{v}\frac{\partial f}{\partial \mathbf{r}} + \left\{\frac{e}{m}\mathbf{E}_{eb} + [\Omega_e, \mathbf{v}] + T_i\frac{\nabla N_1}{N_0}\right\}\frac{\partial f}{\partial \mathbf{v}} = 0 \tag{6}$$

Here Ω_e is electron gyrofrequency and ω_{eb} is frequency of Bernstein wave. The last term $T_i\dfrac{\nabla N_1}{N_0}$ is the ambipolar input of ions, where N_1 is average on oscillations plasma density disturbances and T_i is ion temperature.

To calculate the striction effects it is necessary to solve Eq. (6) taking into account terms of the order of E^2_{eb}. After integrating the distribution function on d^3v, and averaging on oscillations we will find the density perturbations $N1/N0$. Fulfilling this program one can obtain:

$$\frac{N_1}{N_0} = \frac{3}{4m(T_i+T_e)}\left(eE_{eb}\right)^2\frac{\omega_{eb}^2+\Omega_e^2}{\left(\omega_{eb}^2-\Omega_e^2\right)}\sin^2(k_{eb}x) \tag{7}$$

Thus we see that field aligned density perturbations with scale of Bernstein wave would be excited by standing wave due to the action of striction force. As they are much less than the striations, it is naturally to call them super-small-scale (SSS) density perturbations.

Let us estimate now the amplitude of SSS disturbances. According to the theory the amplitude of Bernstein waves is small with respect to upper hybrid waves and could be estimated near *n*-th gyroresonance as [8]:

$$\frac{E_{eb}^2}{E_{uh}^2} \approx \frac{k_{eb}^2\left(n\Omega_e - \omega_{eb}\right)}{k_{uh}^2\left(\omega_{uh} - n\Omega_e\right)}$$

Bearing in mind that due to resonance pumping the amplitude of upper hybrid waves is much higher than the pump wave amplitude E_0 and taking into account the analysis of E_{uh} fulfilled in our previous work [1], one can estimate the amplitude of Bernstein mode $E_{eb}^2 \approx E_0^2$. The estimations of threshold field amplitude (5) near 4-th gyrofrequency, for example, in a frequency shift range 20–80 kHz gives $E_0 \approx 0.3$–0.4 V/m. Thus the mean value of SSS density disturbances (7) could be roughly estimated as:

$$\left\langle \frac{N_1}{N_0} \right\rangle \approx \frac{3e^2E_0^2}{8mT} \approx 0.3\%$$

As one can see from (7) the scale of these disturbances is of the order of k_{eb}^{-1}. In reality they are strongly elongated along the magnetic field and have cylindrical symmetry. In Quarter II we have considered a two dimensional model. We suppose that the super-small scale (SSS) disturbances are located randomly inside striations and have profile

$$\delta N(r_\perp) \propto \exp\left[-\left(k_{eb}r_\perp\right)^2\right]$$

The drifts of perturbations are small and we can consider SSS as stationary. In this proposition the fluctuation spectrum depending on perpendicular to the Earth magnetic field wave vector $k_\perp$ has a form:

$$\left|\frac{\delta N\left(k_\perp\right)}{N}\right|^2 = \left\langle \left(\frac{N_1}{N_0}\right)^2 \right\rangle \frac{P}{4k_{eb}^4} \exp\left\{-\frac{k_\perp^2}{2k_{eb}^2}\right\} \qquad (9)$$

Here *P* is a filling factor of SSS disturbances. To estimate this factor it is necessary to remind that SSS disturbances are excited and packed inside striations, the scale of striation across magnetic field $l_s \approx$ 3-10 m. Hence the number of small-scale perturbations is of the order of square of their scales. Thus the factor *P* could be estimated as:

$$P \approx \left(l_s k_{eb}\right)^4$$

The value of perpendicular wave vector k_{eb} as a function of frequency shift $\Delta_\omega = \omega_0 - n\Omega_e$ from *n*-th resonance could be obtained using dispersion relation (3):

$$k_{eb}\rho_e = \left[\frac{2^{n+1}n!}{n^2-1}\frac{\Delta_\omega^2}{\omega_{pe}^2}\right]^{1/(2n-2)}, \qquad n = 3,4,5,6,..... \qquad (10)$$

To estimate the value of k_{eb} let us choose the typical frequency shift $\Delta_\omega = 0.01\omega_{pe}$. The fluctuation spectrum (9) for different *n* is shown in the Fig.2.1. For example, the value for *n*=4 is $k_{eb}\rho_e = 0.42$.

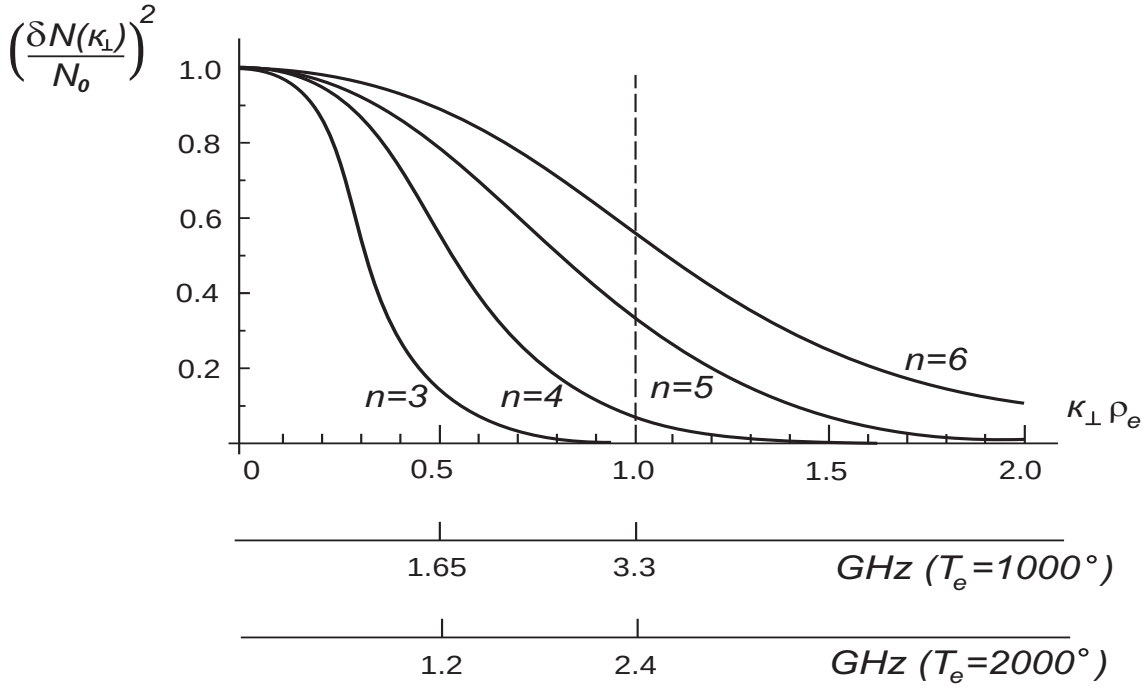

$$\left(\frac{\delta N(\kappa_\perp)}{N_0}\right)^2 = \frac{\sigma}{\sigma_{max}}, \qquad \sigma_{max} = 10^7\ m^2$$

Fig.2.1. The fluctuation spectrum $\left|\delta N / N_0\right|^2$ as a function of $k_\perp \rho_e$ for multiple gyroresonances n=3, 4, 5, 6. Below: two axes in GHz for different electron temperatures.

The field aligned scattering at SSS perturbations is proportional to $\left|\delta N / N_0\right|^2$. One can indicate the following main features of this scattering.

1. Frequency range

Characteristic scattering frequency for *n*-th multiple gyrofrequency is $f_{nc} = ck_{eb}/2\pi$, where k_{eb} is the perpendicular wave vector determined according to (10). Taking a typical frequency shift value $\Delta_\omega = 0.01\omega_{pe}$, we find:

$$f_{nc} = 3.3\left(k_\perp \rho_e\right)\text{GHz}, \quad \text{for } T_e = 1000^0,$$
$$f_{nc} = 2.4\left(k_\perp \rho_e\right)\text{GHz}, \quad \text{for } T_e = 2000^0$$

The frequency dependence is shown at the Fig.2.1. We see that for *n*= 4 ÷ 6 resonances the typical scattering range is up to 2 ÷ 3 GHz.

2. Maximal value of scattering crossection.

From the estimated value of density disturbances (8) one can find the density fluctuations as

$$\left\langle \left(\frac{\delta n}{N_0}\right)^2 \right\rangle \approx 10^{-5}. \qquad (11)$$

Taking into account that for usual striations $\sigma_{\max} \approx 10^8$ m^2 [9, 10] is reached at $(\delta n/n)^2 \approx 10^{-4}$, we estimate the SSS field aligned maximal crossection as $\sigma_{\max}(SSS) \approx 10^7$ m^2.

3. Frequency spectrum

As is well known the field – aligned frequency spectrum width for a wave scattered by usual striation is extremely narrow ~ 0.5 Hz. That demonstrates a high stability of the whole striation structure developed in ionospheric modification.

The width of frequency spectrum for the SSS scattering could be different. According to nonlinear theory there is a strong heating of electrons inside striations [1]. In average: $\langle \Delta T_e \rangle \approx 0.5 T_e$. It means that one can expect a significant drift motion of SSS fluctuations in the direction perpendicular to magnetic field **B**:

$$\mathbf{u}_d = -\frac{1}{m\Omega_e}\left[\frac{\mathbf{B}}{B}, \nabla T_e\right]. \qquad (12)$$

Taking the typical scales of striations l ~10 m [11], one can obtain from (12) $\langle u_d \rangle \approx 5\times 10^3$ cm/s and the typical scattering frequency width is

$$\Delta f \approx \frac{u_d}{c} f_0 \approx 200\left(\frac{f_0}{1\,\text{GHz}}\right)\text{Hz}. \qquad (13)$$

Thus the frequency spectrum width for field aligned scattering of UHF radio waves at SSS is a few hundred Hz.

4. The growth and decay of SSS scattering

Let us consider the scattering process in the case of sharp put on or put off powerful pump wave.

After the put on of the pump wave the striations and SSS are growing together. It means that the characteristic growth time of SSS scattering is of the order of a few seconds – the same as the scale time of striation growth.

Quite a different picture is for decay time. Striations disappear as usually in a few seconds, but SSS density inhomogeneities are created by striction forces and have a very small scales $r_\perp \sim (3-5)$ cm. The plasma diffusion in such scales goes fast: the fluctuations of electrons disappear due to diffusion along inhomogeneities and ions – due to free motion across. It gives the life-time

$$\tau_{\|e} \sim \frac{l_\|}{2D_e} \approx 5\times 10^{-2}\text{ s}, \qquad \tau_{\perp e} \sim \frac{r_\perp}{V_i} \approx 10^{-4}\text{ s}.$$

So the life-time of SSS after the pump put off is only 50 ms or less.

Comparison with the experiment

According to the earlier elaborated theory powerful radio waves which frequency is close to the multiple gyro resonance being used to effect ionosphere produce super narrow striations elongated along the Earth's magnetic field direction. According to our suggestion the experiment devoted to the search for such inhomogeneities was realized at HAARP during 2008 spring campaign. The ionosphere heating was done under the conditions corresponding to the third gyro resonance. The GPS signal from the satellite transited over the HAARP in the experiment moment was used as a diagnostic one. The phase shift of the high-frequency radio signal was observed. The data are processed now.

We have proceed the analysis of the phase shift of the GPS signal from the satellite transiting above the zone exited in ionosphere by the powerful radio wave having frequency close to the third gyro resonance. The data analysis shows that the phase shift sharply changes and even oscillates with the period about 20 s just after heating switch on. This phenomenon

was observed in four of the six sets of observations. The electron density perturbation has a huge value – about 20-40 %. The presence of such strong long scale (1-5 m) perturbations is unlikely from the theoretical point of view. Apparently, effect is connected with the dispersion of the GPS signal on the super small scale irregularities.

The processing of HAARP experimental data was finished. The experiment was devoted to find the scattering of the GPS signal by the electron density perturbations in the F_2 region of the ionosphere. The effect was earlier predicted in the Project. The experiments were conducted using the HAARP heater having the radiating frequency f which matches $3f_B$, i.e., triple the local electron gyro frequency. Such frequency is expected to generate super small irregularities of the electron density which can scatter GPS signals. It was found that the differential phase of the probe GPS signals changed abruptly in about 10 s after the start of the HF-heating, and then oscillated with the heating period 20 s. The oscillations lasted for 4–5 minutes and then disappeared, presumably when the resonance condition $f = 3f_B$ was not satisfied, although the HF-heating continued.

The smallest scale resolvable in the GPS phase data are of an order of tens of meters given the scan velocity of the GPS beam in the F_2 region and the 2 Hz sampling rate. Thus the experiment does not provide a direct proof that the observed GPS perturbations are caused by super small scale (SSS) irregularities such as predicted by the theory. However, there are some indications that SSS irregularities play a role in this effect as discussed below.

In fact, let us estimate the phase change due to GPS signals of frequency ω passing through the perturbed region of the ionosphere:

$$\Delta\phi = \frac{\omega}{c}\int \varepsilon dz \approx \frac{\omega}{c}\frac{\omega_e^2}{\omega^2}\frac{\delta n}{n} I$$

where ε is the refraction index, $\omega_e = (4\pi e^2 n/m)^{1/2}$ is the electron plasma frequency, δn is the electron density perturbations due to the HF-heating, and I is the length of the perturbed region. For the heating frequency equal to 4.3 MHz, and assuming that $\omega_e \approx 2\pi \times 4.3 \times 10^6$ s^{-1} it could be obtained that

$$\frac{\delta n}{n} \approx \frac{10\Delta\phi(rad)}{I(km)}$$

The differential phase observed in the experiment was about 0.1 radians, while the width of the disturbed region does not exceed 5–10 km. This gives the electron density perturbations of 10 – 20% which is almost an order of magnitude higher than that usually observed. Such enormous phase perturbations occurring on a one-second timescale indicate that scattering of GPS signals by the SSS irregularities could contribute to the differential phase observed.

Beside the abrupt relaxation of STEC perturbations detected in experiments (see the pulses marked by the arrows on Figure 2.2 (bottom)), shows that STEC relaxes to its unperturbed value within a fraction of a second after the termination of the HF pulse. The fast relaxation implies that it is caused by the ponderomotive force associated with the SSS irregularities, since the relaxation of the large scale irregularities occur on a much longer timescale. Apparently no other process in the ionosphere can lead to such fast scattering of GPS signals.

Thus, the observed phase oscillations indirectly indicate the presence of super small scale irregularities of electron density produced by the HF heating at the frequency corresponding to $3f_B$.

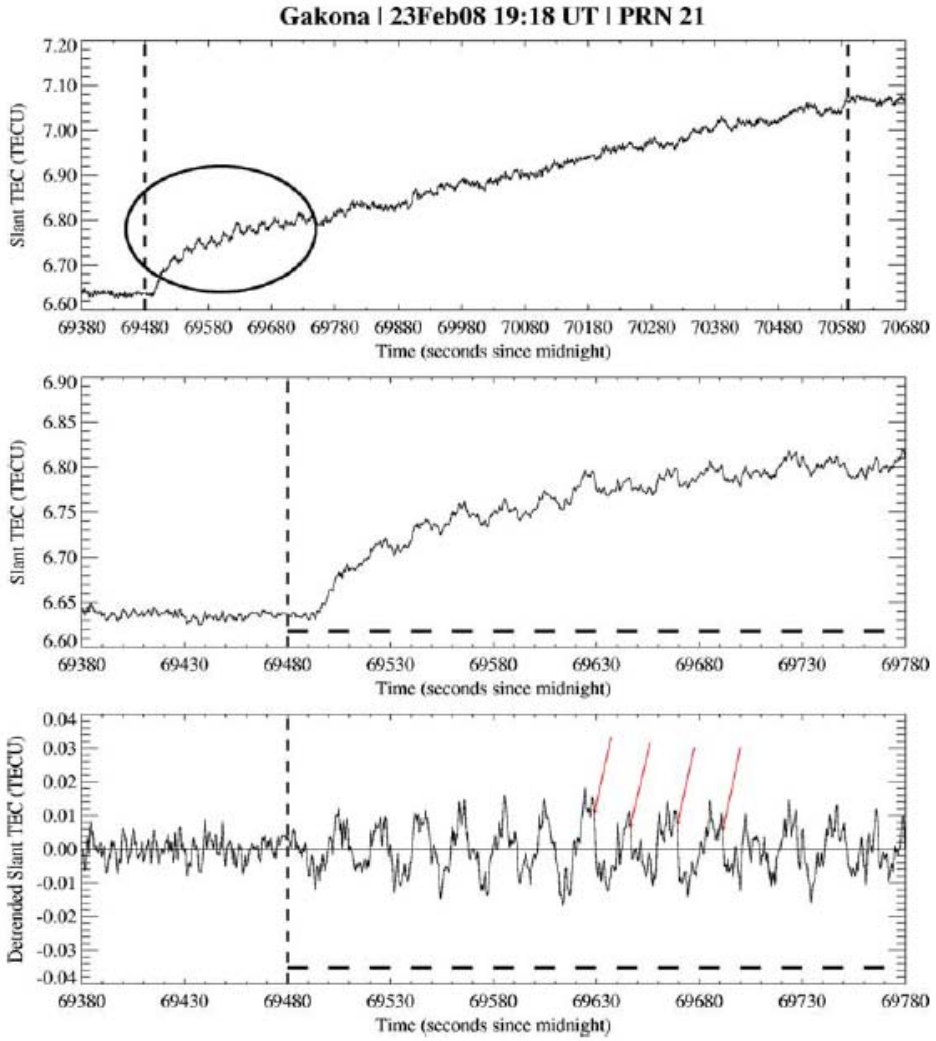

Figure 2.2 (top) Absolute STEC versus the observational time is revealed. The encircled area shows oscillations with 20 s period. (middle) The 5 minutes period of STEC oscillations is zoomed, while (bottom) the de-trended STEC during the same period is shown. The beginning and end of the HF-heating are marked by the vertical dashed lines. The black horizontal bars show the heating periods, each is 10 s long.

References

1. Gurevich A.V., A.V.Lukyanov, K.P.Zybin Phys.Lett.A., 211, 363, 1996
2. Stubbe P., J.Atmos.Terr.Phys. 58, 349, 1996.
3. Bernhardt P.A., M.Wong, J.D.Huba, B.G.Fejer, L.S.Wagner, J.A.Goldstein, C.A.Selcher, V.L.Frolov and E.N.Sergeev J. Geophys. Res., 105, A5 10657, 2000.
4. Grach S.M, B.Thide, T.B.Leyser Radiophys. Quantum Electr. 37, 392, 1994.
5. Bud'ko N.I, V.V.Vas'kov, Geomagn.Aerom. Engl. transl. 32, 63, 1992.
6. Zhou H.L, J.Huang, S.P, Kuo, Phys. Plasma 1, 3044, 1994.
7. Leyser T., B.Thide, H.Derblom, A.Hedberg, B.Lundborg, P.Stubbe, H.Kopka, JGR 95, 17233, 1990.
8. Huang J., S.P.Kuo, JGR 99, 19569, 1994.
9. P.S.Failer, Radio Sci. 9 (1974) 923.
10. J.Minkoff, Radio Sci. 9 (1974) 997.
11. M.C. Kelley, T.L. Arce, J. Salowey, H. Sulzer, W.T. Armstrong, M. Carter, L. Duncan, J. Geophys. Res. 100 (1995) 17367.

Task 3: Generation of powerful gamma emission, powerful bipolar radio pulses and optic emission from the high-altitude thunder discharges. Theoretical investigation, comparison with the existing observations and plans of future experiments

The theory of the high-altitude atmosphere discharge was developed conformably to the combined action of the runaway breakdown (RB) and extensive atmosphere shower (EAS) in thunderstorm electric field. EAS can be initiated at the heights 13-20 km only by particles propagating with small angle to the horizon. EAS weight can reach one kilometer. It was shown in the developed model that runaway breakdown is essentially amplified under these conditions.

Introduction

Runaway breakdown in air (RB) is stimulated by the presence of high energy cosmic ray secondaries. Extensive atmospheric showers (EAS) are accompanied by an effective local growth of the number of cosmic ray secondaries and thus have a strong influence on the RB process [1]. The combined action of runaway breakdown and EAS lead to the development of RB–EAS discharge – the discharge where relativistic electrons play a decisive role. RB-EAS discharge is accompanied by strong exponential growth of the number of energetic and thermal electrons, positrons and gamma quanta [2]. It can serve for the generation of a strong bipolar radio pulse [3].

A distinct class of radio pulses generated in thunderstorms was effectively studied during recent years in observations of Smith et al [4-6]. These studies allowed establishing that the radio pulses having enormous peak power up to 100 GW are emitted in the wide frequency range by the intracloud discharges in the tropopause. The pulses are short time (≤ 10 μs) and have a definite bipolar form. That is why they were called narrow bipolar pulses (NBP). The observations show that these strong radio pulses are isolated – not accompanied by usual lightning leader and return stroke. Their optic emission is very weak. A detailed analysis of the whole complex of observational data allowed Jacobson (2003) to state that NBP is a new type of thunderstorm discharge quite different from usual lightning [7]. He speculated that it could have relevance to runaway breakdown effect.

A theory of RB-EAS discharge in air was compared with the results of NBP observations and qualitative agreement was demonstrated [8]. That allowed to state that RB–EAS discharge can serve as a background of NBP phenomena. Note, that in [8] a simplified model where a high energy cosmic ray particle moving along the vertical direction parallel to the thundercloud electric field E was used.

In the same time the NBP are generated at tropopause heights (10–20) km. At such a high heights energetic cosmic ray (CR) particle has a well developed extensive atmospheric shower (EAS) only if its momentum has a large angle θ to the vertical direction $\theta > 60^o - 70^o$ [9]. The first goal of our investigation is to develop a theory which takes this fact into account. We will demonstrate that inclination of CR particle trajectory lead to elongation of the path of runaway breakdown what serves for significant amplification of RB. It means that the RB-EAS discharge current grows effectively with the inclination angle θ and in NBP conditions can reach extremely high values – up to 100 kA and even more.

Note that in the considered previously RB–EAS discharge models the electric field in thundercloud was supposed to be a given stationary function of height z [2, 8]. That is correct for not too strong current only. Let us remind that the energy spent during RB - EAS discharge comes from the electrostatic energy of thundercloud electric field. This is the only energy source. It is evident that if the discharge is intensive enough a part of electrostatic energy is dissipated and the electric field in the cloud should diminish. This will affect the RB –EAS discharge and determine its nonlinear modification.

The second goal of the investigation is to develop the RB–EAS discharge theory taking into account nonlinear process. We will demonstrate that high power discharges are strongly modified due to this nonlinearity.

RB - EAS discharge at tropopause heights

Extensive atmospheric shower (EAS) becomes well developed when the energetic cosmic ray (CR) particle pass a significant length τ in the atmosphere $\tau > \tau_\varepsilon$ [12]. Here:

$$\tau = \frac{1}{\cos\theta}\int_z^\infty \rho(z)\,dz$$

is the integral of atmospheric density $\rho(z)$ measured in g/cm^2 and θ is the inclination angle of CR particle having energy ε. The radiation length τ_ε is growing with energy logarithmically

$$\tau_\varepsilon = \ln\left(\frac{\varepsilon}{80\text{MeV}}\right)\ \text{g/cm}^2$$

and for $\varepsilon = 10^{16} - 10^{19}$ eV takes the value $\tau_\varepsilon = 18.5 - 25.4$.

Atmosphere at the heights of NBP generation (10–20) km is not dense. For example in the case of vertically moving CR particle for the height z = 16 km the integral length is only τ = 5 g/cm2. That is why EAS become well developed only if the energetic cosmic ray particle momentum is directed close to the horizon $\theta_h = 90^o - \theta < \theta^*(\varepsilon)$. The critical angle θ^* for the height z = 16 km is presented in the Table 1.

Table 1. EAS critical angles

ε (eV)	θ^*_{degree}	θ^*_{rad}
10^{16}	16^o	0.28
10^{17}	14^o	0.24
10^{18}	12.5^o	0.22
10^{19}	11.4^o	0.20

Taking the electric field in the thundercloud directed as usual close to the vertical one can see that now the RB - EAS discharge is developing in quite a new condition. In models considered previously the CR particle momentum was always supposed to be directed along the vertical axis z [2], [8] what automatically lead to the development of the discharge along electric field E_z with the velocity of light c. Now the CR particle is moving practically perpendicular to E. How will the RB–EAS discharge develop in these conditions?

First we have to remind that to realize RB two conditions are needed:

– a seed high energy ($\varepsilon > 0.5$ Mev) electrons,

– the electric field $E > E_c$ in the thundercloud.

The first condition is fulfilled for EAS because it generates a large number of high energy electrons having a widely spread angular distribution in energy region $\varepsilon \le 1$MeV [4, 12, 13]. Namely this energy region is the most interesting for excitation of RB. So we see that if $E > E_c$ the both requirements are fulfilled and RB–EAS discharge exists in the considered new conditions.

But there is a specific discharge peculiar property, different from the previous case $v \| E$. It is plotted qualitatively at the Fig.3.1. In Fig.3.1 the CR particle is shown moving along x−axis. Electric field is directed up along z perpendicular to x. The RB process begins from point $x = 0$ and $z = z_c$ where $E(x,z) > E_c$ and goes down along z-axis. It is shown by the arrows. The velocity of RB region boundary in z direction is determined by distribution function of runaway electrons in the energy region ε~0.3−0.5 MeV. According to numerical calculations Symbalisty et al [12], Lehtinen et al [13] the average directed velocity $\langle v_z \rangle$ in this region is

$$\langle v_z \rangle = 2\pi\int v\mu f(v,\mu,t)v^2 dv d\mu \approx (0.3-0.5)c \qquad (1)$$

We see that $\langle v_z \rangle$ is significantly less than c. Due to this as the RB growth time τ_{rb} depends on E/E_c only (see [14]) the RB effective avalanche length

$$l_{aeff} = \langle v_z \rangle \ \tau_{rb} \qquad (2)$$

is diminishing. This diminishing of effective avalanche length l_{aeff} lead to exponential amplification of RB–EAS discharge in a given thundercloud electric field layer L ($\propto exp(L/l_{aeff})$). Another significant amplification process is connected with the growth of EAS cross section which is determined by the diminishing of electron energy losses at tropopause heights due to low density of air molecules.

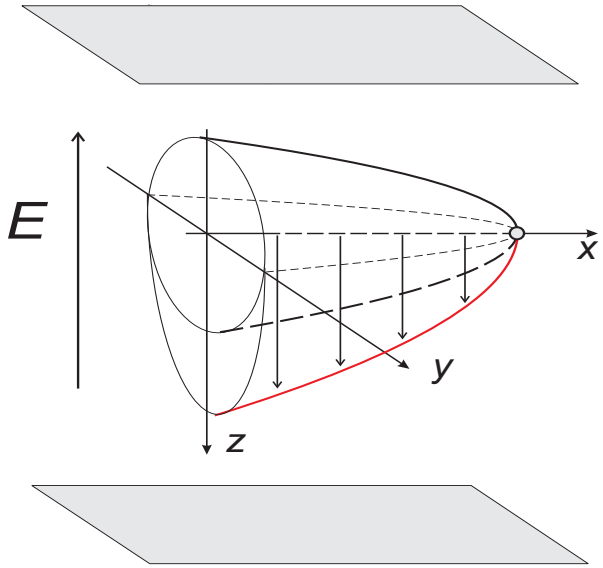

Fig.3.1

The kinetic theory of gamma emission propagation in non-uniform atmosphere was developed. The goal of the investigation is to clearify the nature of TGFs, gamma-bursts registered on the satellites COMPTON and RHESSI as comming from the Earth. The emission was found to be assotiated with lightning.A theoretical model of gamma radiation propagation and its yeild from the non-uniform Earth atmosphere is needed to estimate radiation parameters in the source. The kinetic equation discribing the photon propagation was obtained for the case of arbitrary nonunniform media. In the commoncase it has the form:

$$\frac{\partial n(\mathbf{r},\mathbf{k},t)}{\partial t}+c\frac{\mathbf{k}}{k}\frac{\partial n(\mathbf{r},\mathbf{k},t)}{\partial \mathbf{r}}=\left(\frac{\delta n}{\delta t}\right)_{ph,e}$$

where $n(\mathbf{r},\mathbf{k},t)$ – photon density in the phase space $(\mathbf{r},\mathbf{k})$, $\left(\frac{\delta n}{\delta t}\right)_{ph,e}$ – photon–electron collision integral.

$$\left(\frac{\delta n}{\delta t}\right)_{ph,e}=\int\left(f(\mathbf{p}')n(\mathbf{k}')[1+n(\mathbf{k})]-f(\mathbf{p})n(\mathbf{k})[1+n(\mathbf{k}')]\right)\times \tag{1}$$

$$\times\omega(\hat{\mathbf{p}'},\hat{\mathbf{k}'},\hat{\mathbf{p}},\hat{\mathbf{k}})d^3pd^3p'd^3k',$$

here $\omega(\hat{\mathbf{p}'},\hat{\mathbf{k}'},\hat{\mathbf{p}},\hat{\mathbf{k}})$ – the probability of the photon transition from the state with impulses $(\mathbf{p},\mathbf{k})$ into the state with impulses $(\mathbf{p}',\mathbf{k}')$. In the relativistic invariant form this probability could be written as:

$$\omega(\hat{\mathbf{p}'},\hat{\mathbf{k}'},\hat{\mathbf{p}},\hat{\mathbf{k}})=\frac{e^4}{2}R\frac{\delta(\hat{\mathbf{p}}+\hat{\mathbf{k}}-\hat{\mathbf{p}'}-\hat{\mathbf{k}'})}{\varepsilon\varepsilon' kk'},$$

$$R=\left(1+\frac{m^2}{A}-\frac{m^2}{B}\right)^2+\frac{A}{B}+\frac{B}{A}-1.$$

ε – electron energy, A X B – kinematic invariants:

$$A=\hat{\mathbf{k}}\hat{\mathbf{p}}=k(\varepsilon-pcos\xi)\equiv\hat{\mathbf{k}'}\hat{\mathbf{p}'},$$

$$B=\hat{\mathbf{k}'}\hat{\mathbf{p}}=k'(\varepsilon-pcos\xi')\equiv\hat{\mathbf{k}}\hat{\mathbf{p}'},$$

After integrating (1) over scattered electron impulses p', and the over the target poton impulses k' the collision integral takes the form:

$$\left(\frac{\delta n}{\delta t}\right)_{ph,e}=\frac{e^4}{2k^2}\int f(\mathbf{p})d^3pd\Omega'\frac{\tilde{R}\tilde{k}^2n(\tilde{\mathbf{k}})[1+n(\mathbf{k})]-Rk'^2n(\mathbf{k})[1+n(\mathbf{k})]}{\varepsilon(\varepsilon-pcos\xi)}, \tag{2}$$

where

$$R=\left[1-\frac{m^2(1-cos\chi)}{(\varepsilon-pcos\xi)(\varepsilon-pcos\xi')}\right]^2+$$

$$+\frac{m^2(1-cos\xi')}{\varepsilon-pcos\xi'+k(1-cos\chi)}+\frac{\varepsilon-pcos\xi'+k(1-cos\chi)}{m^2(1-cos\xi')}-1,$$

χ - the angle between vectors $\mathbf{k}$ X $\mathbf{k}'$, ξ - the angle between vectors $\mathbf{p}$ X $\mathbf{k}$, ξ' - the angle between vectors $\mathbf{p}$ X $\mathbf{k}'$, $\tilde{R}=R(\tilde{k})$, $\tilde{k}$ has the form

$$\tilde{k}=\frac{k(\varepsilon-pcos\xi)}{\varepsilon-pcos\xi'-k(1-cos\chi)}.$$

In the case when the photon energy is much higher then the electron temperature the electron distribution function has the form:

$$f(\mathbf{p},z)=N(z)\delta(\mathbf{p}). \tag{3}$$

Taking (3) into account the expresion (2) could be rewritten as

$$\left(\frac{\delta n}{\delta t}\right)_{ph,e}=\frac{e^4}{2m^2k^2}N(z)\int d\Omega'\left(cos^2\chi-\frac{k}{m}(1-cos\chi)+\frac{1}{1-\frac{k}{m}(1-cos\chi)}\right)\times$$

$$\times\frac{k^2n(\tilde{k},\Omega')}{\left(1-\frac{k}{m}(1-cos\chi)\right)^2}-\left(cos^2\chi+\frac{k}{m}(1-cos\chi)+\frac{1}{1+\frac{k}{m}(1-cos\chi)}\right) \tag{4}$$

$$\times\frac{k^2n(k,\Omega)}{\left(1+\frac{k}{m}(1-cos\chi)\right)^2}$$

We study the case when $\frac{k}{m}\ll 1$, i.e. the photon energy is much less then the electron rest energy. In the first approximation over the ratio of these two energies the photon distribution function does not change in the collision as the function of the wave number value k. It changes only as the function of the scattering angle. Thus (4) could be integrated over k. Finally the kinetic equation have the form:

$$\frac{\partial n}{\partial t}+\frac{\sqrt{1-\mu^2}}{r}\frac{\partial(rn)}{\partial r}+\mu\frac{\partial n}{\partial z}=$$

$$=\frac{3}{8}\sigma_{Th}N(z)\left\langle(3\mu^2\mu'^2-\mu^2-\mu'^2+3)(n(\mu')-n(\mu))\right\rangle_{\mu'}. \tag{5}$$

where $\mu=cos\vartheta$, $\mu'=cos\vartheta'$, ϑ, ϑ' - polar anges of the income and outcome photons respectively.

Function $n(t,r,z,\mu)$ is expanded over Legendre polinoms in order to simplify the collision integral of photons with electrons

$$n(t,r,z,\mu)=\sum_{k=0}^{\infty}n_k(t,r,z)P_k(\mu)$$

After substitution of these expressions into (5) and elementary transformations the sought kinetic equation could be obtained:

$$\frac{\partial n}{\partial t} + \frac{\sqrt{1-\mu^2}}{r}\frac{\partial (rn)}{\partial r} + \mu\frac{\partial n}{\partial z} = \tag{6}$$

$$= \sigma_{Th} N(z)\left(n_0 - n + \frac{1}{10} n_2 P_2(\mu)\right),$$

Here $N(z)$ - the air density, σ_{Th} – the cross-section of the Tomson scatering of the photons on electrons, μ - the cosine of the angle between the photon impulse direction and the non-unifomity gradient, n_0 - photon distribution function averaged over the angles, n_2- photon distribution function intergated together with the second Legendre polinom, $P_2(\mu)$ - second Legendre polinom. Note, that no assuptions about the value of the non-uniformity gradient was done while obtaning the kinetic equation. So, the equation (6) as well as the initial equation (1) is true for the arbitrary value of atmosphere non-unifomity. The analysis of the equation (6) was started. It was shown that its exact solution for the function $n(z, r, \mu, t)$ is completely determined only by the zero and second expansion coefficients of the function over Legendre polinoms.

After substitution of these expressions into (5) and elementary transformations the sought kinetic equation should be obtained:

$$\frac{\partial n}{\partial t} + \frac{\sqrt{1-\mu^2}}{r}\frac{\partial (rn)}{\partial r} + \mu\frac{\partial n}{\partial z} = \sigma_{Th} N(z)\left(n_0 - n + \frac{1}{10} n_2 P_2(\mu)\right) \tag{6}$$

Here the air density changes with the altitude as

$$N(z) = N_0 e^{-az},$$

where N_0 - the electron density at the height $z = 0$, $1/a$ - the characteristic scale of atmosphere density change. σ_{Th} - the cross-section of the Tomson scattering of the photons on electrons, томсоновское сечение рассеяния фотонов электронами, μ - the cosine of the angle between the photon impulse and the non-uniformity gradient, $P_2(\mu)$ – second Legendre polynom. Note, that no assumptions about the value of the non-uniformity gradient was done while obtaining the kinetic equation. So, the equation (6) as well as the initial equation (1) is true for the arbitrary value of atmosphere non-uniformity. The exact solution for the function $n(z, r, \mu, t)$ is completely determined only by the zero and second expansion coefficients of the function over Legendre polynoms.

Introducing a new mark $1/l$ for $\sigma_{Th} N_0$, equation (6) could be transferred to the form:

$$\frac{\partial n}{\partial t} + \mu\frac{\partial n}{\partial z} + \frac{1}{l} e^{-az} n = \frac{1}{l} e^{-az}\left(n_0 + \varepsilon n_2 P_2(\mu)\right). \tag{7}$$

Consider the linear differential operator

$$Ln(t, z, \mu) = \left(\frac{\partial}{\partial l} + \mu\frac{\partial}{\partial z} + \frac{1}{l} e^{-az}\right) n(t, z, \mu) = N(t, z, \mu).$$

The solution of this inhomogeneous partial differential equation could be obtained by the standard Green function method.

$$n(t, z, \mu) = n(0, z, \mu) + \int_0^t \int_{-\infty}^{+\infty} \int_{-1}^{+1} dt' dz' d\mu' G(t, z, \mu; t', z', \mu') N(t', z', \mu'),$$

where $n(0,z,\mu)$ - $n(t,z,\mu)$ at the initial moment ($t=0$), $G(t,z,\mu;t',z',\mu')$ - Green function obeying the following equation

$$\left(\frac{\partial}{\partial t}+\mu\frac{\partial}{\partial z}+\frac{1}{l}e^{-az}\right)G=\delta(t-t')\delta(z-z')\delta(\mu-\mu').$$

Presenting function G as a product $\exp\left(\frac{e^{-az}}{al\mu}\right)g$ one can obtain

$$\left(\frac{\partial}{\partial t}+\mu\frac{\partial}{\partial z}\right)g=\exp\left(-\frac{e^{-az'}}{al\mu}\right)\delta(t-t')\delta(z-z')\delta(\mu-\mu').$$

Now transforming g as $\exp\left(-\frac{e^{-az'}}{al\mu}\right)\chi$, where χ obey the equation

$$\frac{\partial\chi}{\partial t}+\mu\frac{\partial\chi}{\partial z}=\delta(t-t')\delta(z-z')\delta(\mu-\mu'),$$

Its solution has the form

$$\chi=\theta(t-t')\delta(z-z'-\mu(t-t'))\delta(\mu-\mu').$$

It means that the Green function is equal to

$$G(t,z,\mu;t',z',\mu')=\exp\left(\frac{e^{-az}-e^{-az'}}{al\mu}\right)\times$$
$$\times\delta(z-z'-\mu(t-t'))\delta(\mu-\mu')\theta(t-t'), \qquad (8)$$

Thus, the differential equation (7) could be rewritten as the integral equation

$$n(t,z,\mu)=n(0,z,\mu)+\frac{1}{l}\int_0^t\int_{-\infty}^{+\infty}\int_{-1}^{+1}dt'dz'd\mu'\exp\left(\frac{e^{-az}-e^{-az'}}{al\mu}-az'\right)\times$$
$$\times\delta(z-z'-\mu(t-t'))\delta(\mu-\mu')\left[n_0(t',z')+\varepsilon n_2(t',z')P_2(\mu')\right]. \qquad (9)$$

The analysis of equation (9) allowed to find the form of the photon distribution function on condition that $\hbar k/mc>>1$, where *k*- photon momentum. The distribution function is found as a function of an angle, time and height. The form the function for different values of parameter *az* and time moments *at* is shown in Fig. 3.2.

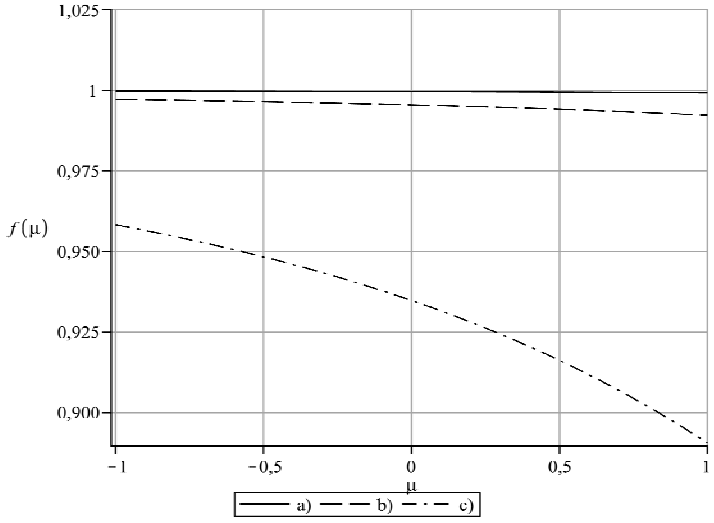

Fig.3.2. $f(t,z,\mu)$ as the function of μ at: a) $az=10$, $at=1$, $al=0.1$; b) $az=10$, $at=1$, $al=0.01$; c) $az=5$, $at=1$, $al=0.1$.

The angle dependence of the photon density $n(t,z,\mu)$ is determined by the function $\theta(\mu)=\rho+\mu^2$,

where $\rho = \frac{20}{\chi_2^2}\left(2 - \frac{3\chi_2^2}{70}\right) \approx 2.8,$

This implies that the preferential direction in the photon propagation iz along the axis of inhomogenity Oz towards the less medium density (Fig.3.3).

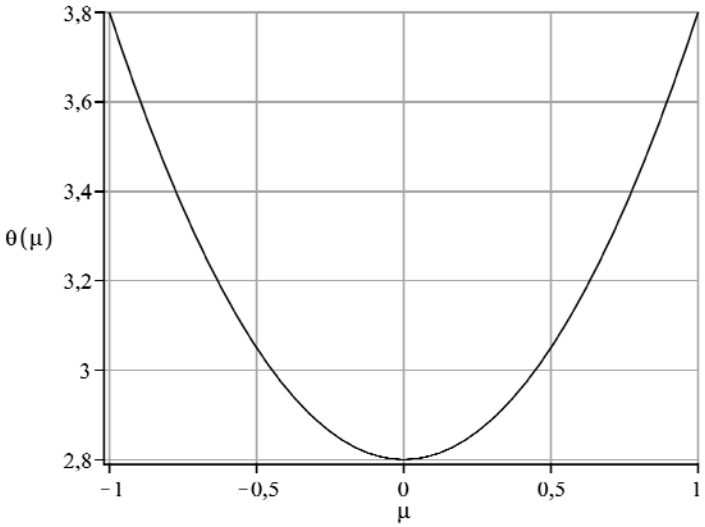

Fig.3.3. Plot of $\theta(\mu)$.

References

1. A.V.Gurevich, K.P.Zybin, R.A.Roussel-Dupre Phys.Lett. A **254**, 79 (1999).
2. A.V.Gurevich, Yu.V.Medvedev, K.P.Zybin Phys.Lett. A **329**, 348 (2004).
3. A.V.Gurevich, L.M.Duncan, Yu.V.Medvedev, K.P.Zybin Phys. Lett. A **301**, 320 (2002).
4. D.A.Smith, X.M.Shao D.N.Holden, C.T. Rhodes, M Brook, P.R.Krehbiel, M.Stanley W.Rison, R.J.Thomas J. Geophys. Res. **104**, 4189 (1999).
5. D.A.Smith K.B.Eack J.Harlin, M.J.Heavner, A.R.Jacobson, R.S.Massey, X.M.Shao, K.C.Wiens J.Geophys.Res **107**, D134183 (2002).
6. D.A.Smith, M.J.Heavner, A.R.Jacobson, X.M.Shao, R.S.Massey, R.J.Sheldon, K.C.Wiens Radio Sci. **39**, N1, RS1010, (2004).
7. A.R.Jacobson J.Geophys.Res **108** D244778 (2003).
8. A.V.Gurevich, K.P.Zybin Phys.Lett. A **329**, 341 (2004).
9. V.S.Murzin, Physics of Cosmic Rays, Moscow, Univ. Press (1988); T.K.Gaisser, Cosmic Rays and Particle Physics, Cambrige U. Press, New York (1990).
10. E.M.D.Symbalisty, R.A.Roussel-Dupree, V.B.Yuhimuk IEEE Trans. Plasma Sci. **26**, 1575 (1998).
11. N.G.Lehtinen, T.F.Bell, U.S.Inan J. Geophys. Res. **104**, 24699 (1999).
12. E.M.D.Symbalisty, R.A.Roussel-Dupree, V.B.Yuhimuk IEEE Trans. Plasma Sci. **26**, 1575 (1998).
13. N.G.Lehtinen, T.F.Bell, U.S.Inan J. Geophys. Res. **104**, 24699 (1999).
14. A.V.Gurevich, K.P.Zybin Physics – Uspkchi **44**, (11), 1119 (2001).

Task 4: High-energy particles in thunder (lightning) phenomena. Experimental and theoretical investigation of intensive gamma emission, generation of HF and VHF radio waves, electric field, electric field variations

Experiment

DISCRIPTION OF THE THUNDERSTORM COMPLEX

The experimental complex "Thunderstorm" is located at the height 3340 m above the sea level. It consists of the following installations: storm trigger system, scintillation system of NaI-detectors, multi-layers spectrometer of absorption, muon hodoscopes, monitoring system of high-energy and thermal neutrons, two independent radio systems working in a range of frequencies 0,1 - 30 MHz and ~ 250 MHz, detector of jump of a static electrical field and its high-frequency component. All experimental complex works continuously from the moment of start (April) before ending a season of thunderstorms (September) in an automatic mode.

The storm trigger system consists of several tens detectors created on the basis of Geiger counters SI5G. This system fixes the moment of extensive atmosphere showers of cosmic rays (EAS) passage, allows estimating its size, and also energy of a primary particle. One EAS detector consists of 20 counters SI5G, and its sensitive area is about 0,6 m^2. The EAS trigger detectors are covered with iron filter 10 cm width (Fig.4.2) in order to exclude accidental coincidences induced by low-energy (below 10 MeV) electrons.

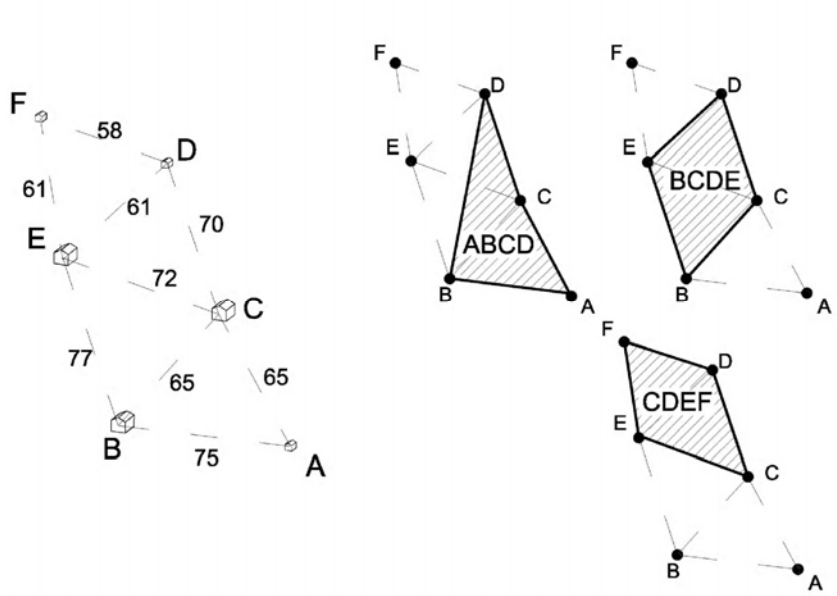

Fig.4.1. Relative location of EAS triggers registration points.

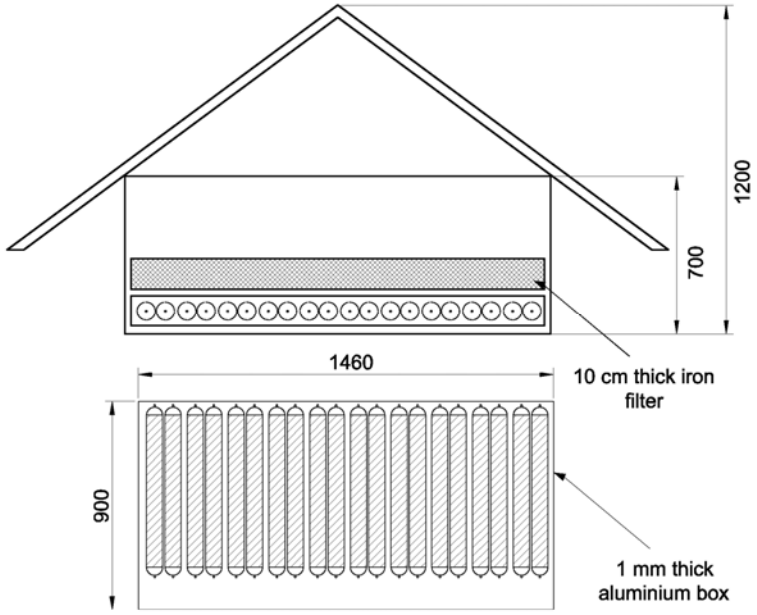

Fig.4.2. EAS trigger system detectors.

The EAS trigger is produced when the pulses from four neighbor registration points coincide in time. The scheme of the trigger formation is presented in Fig.4.3.

The computer modeling showed that such configuration of EAS trigger system provides the effective selection of EAS having primary energy higher than 1 PeV and which axes cross the system at the distance up to 100m.

The scintillation system from 14 scintillation NaI-detectors is used for registration of intensity of soft γ and x-ray radiation from thunderstorm clouds. Detectors are situated in pairs in 7 registration points build on the Tyan-Shan Station pass and on the flanks of surrounding hills. They are placed as a chain (see Fig.4.3) perpendicular to the usual direction of the thundercloud movement. The distance between the extreme points in this chain is about 2 km, the vertical interval occupied by the registration points is about 500 m. Thus the "Thunderstorm" scintillation system allows studying directly the space distribution of the emission inside thunderclouds both in horizontal and vertical directions.

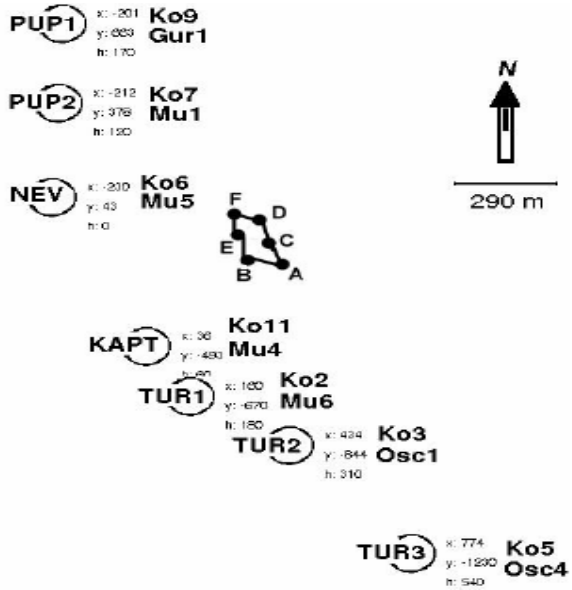

Fig.4.3. Location of the NaI scintillation detectors on the Tyan-Shan Station pass.

Two scintillation detectors are situated in each registration points. NaI crystal in one of this detector is placed inside the metal (aluminum, 1 mm) case. The case of the second detector is done of a bit of the polyethylene pipe with wall thickness 10mm. As a result two detectors have different gamma emission registrations thresholds. In addition in each registration points most distant from the center (PUP1, PUP2, TUR2 и TUR3 on the Figure) one “empty”, without NaI crystal, detector is placed. The signals of “empty” detectors are linked to the joint registration system. They serve for the control of electromagnetic breakthroughs on cables connecting the registration points with the data control center.

Pulses with standard amplitude (TTL compatible) formed by comparators are 5 μs long. They are transferred to the data registration system based on CAMAC. The system provides recording of signal intensity during 4000 time intervals having duration 200 μs each. This system operates continuously. It keeps in memory the intensity time dependence for last 0.8 s. When the special control signal, the trigger, come the data registration system continues its work for 0.4 s. After that the data accumulated are recorded on the disk. Thus, the time dependence of signal intensity is recorded with 200 μs resolution during 0.4 s after the trigger moment.

The absorption spectrometer consists of layers SI5G counters alternated by thin layers Pb and Fe. Absorption spectrometer is used as for the registration of electrons accelerated in thunderstorm electric field as for the registration of γ-emission from these electrons. The energy of electrons and γ-quanta is estimated as well.

«THUNDERSTORM» complex includes «Radio-HF» installations for radio emission waveform measurements in the frequency range of 0,1 – 30 MHz and «Radio-E» installation to measure electric field and its variations.

«Radio-HF» installation is designed to record short (down to 30 ns) electromagnetic pulses generated in thunderclouds by lightning discharges and their sources direction finding. It consists of three spaced (by about 70 m) antenna assemblies, connected to central recording unit by cables of equal length. Each antenna assembly contains three antennas: two crossed by 90° loops to measure horizontal magnetic field component, and End-Fed antenna to measure vertical component of electric field.

The complex includes two such installations spaced by about 400 m that provides a possibility to determine radio emission source location at distances up to 2 – 4 km. Radio installations operate in the external trigger mode. The overall record duration was 200 ms with prehistory time 160 ms (record time duration before the trigger coming).

«Radio-E» installation is designed to record electric field under thunderstorm conditions, its variations is the frequency range 0.5–25 kHz and 250 MHz radio emissions. It also produces the drive pulse when the amplitude of electric field variation overrides the threshold value. Static ("slow") electric field is measured by electrostatic flux meter ("field mill" type). Electric field variations («fast» field) are measured using capacitor type sensor. At the lightning discharge moment «Radio-E» equipment registers static electric field change, its fast variations (stepped leader and return stroke for cloud-to-ground discharges), and form a control signal (lightning trigger) for other installations of the experimental complex. The installation uninterruptedly registers data in the "slow" mode with the frequency of 20 Hz. After the first drive pulse is produced it turns into the "fast" registration mode. In this mode the data digitization rate is 20 μs during one hour, after that the installation turns back to the "slow" mode.

Data processing

The database containing events registered at the Tien-Shan Mountain Station during 2007 summer observation campaign was created. It is based on the MySQL 5.1 SQL-server and use OpenOffice.org 2.4 as a SQL-client. For each registered event the following data were put in:

1. date;
2. time;
3. registration of short wave radio emission (SW);
4. registration of electric field jump;
5. registration of gamma emission;
6. registration of gamma emission spectrum;
7. the type of the trigger (EAS, fast electric field jump, electromagnetic pulse) initiated the record;
8. the estimation of the electric field jump;
9. qualitative estimation of the gamma emission (weak or strong);
10. registration of the noise in control gamma registration channels;
11. registration of SW emission by each of Radio-1 and Radio-2 installations;
12. registration of the electric field jump;
13. registration of gamma emission in each of the observation points TUR1, TUR2, TUR3, KAP, PUP1, PUP2, NEV.

All the events registered during the thunderstorm activity on 08/01, 08/02, 08/03, 08/04, 08/07, 08/08 and 08/25, 2007 are placed in the database.

Registered events, total Including:	169 0
Caused by the electromagnetic pulse trigger	968
Caused by the EAS trigger	686
Caused by the fast electric field jump trigger	36

The small number of fast electric field jump trigger events is determined by the high threshold for this trigger fixed in 2007.

The selection of the similar events for the purpose of the further analysis was done using database. Numbers of events in the selected groups are presented in the Table.

Electromagnetic pulse trigger + SW emission is registered	601
EAS trigger + gamma emission is registered	623
EAS trigger + gamma emission is registered + spectrum of gamma emission is	49

registered	
EAS trigger + SW emission is registered	36
EAS trigger + gamma emission is registered + SW emission is registered	29
Gamma emission is registered + electric field jump is registered	192
Gamma emission is registered + gamma emission is registered + SW emission is registered	131
Strong gamma emission is registered + SW emission is registered	115
Gamma emission is registered in two or more registration points	685
Strong gamma emission is registered in two or more registration points	512

The Section THUNDER of the site http://www.tien-shan.org/she/vardbaccess/ was developed (in Russian). This Section contains the time scans of radio emission registered in 2007 in all registration points as well as the observation log. Fast view of the gamma emission at registration points TUR1, TUR2 и TUR3 is available.

The data processing showed up the short gamma flashes events having complex structure: 10-30 MeV electrons; low energy (dozens keV) and high energy (~MeV) gamma quanta. There is a temporary correlation of short-term flashes with the moments of the lightning registered by electromagnetic pulse trigger. The spatial correlation of these flashes of radiation with the presence of thunderclouds nearby the experimental setup location is found. The spatial sizes of area of flare are about hundred meters. Probably this type of events is connected with cloud-to-cloud electric breakdown.

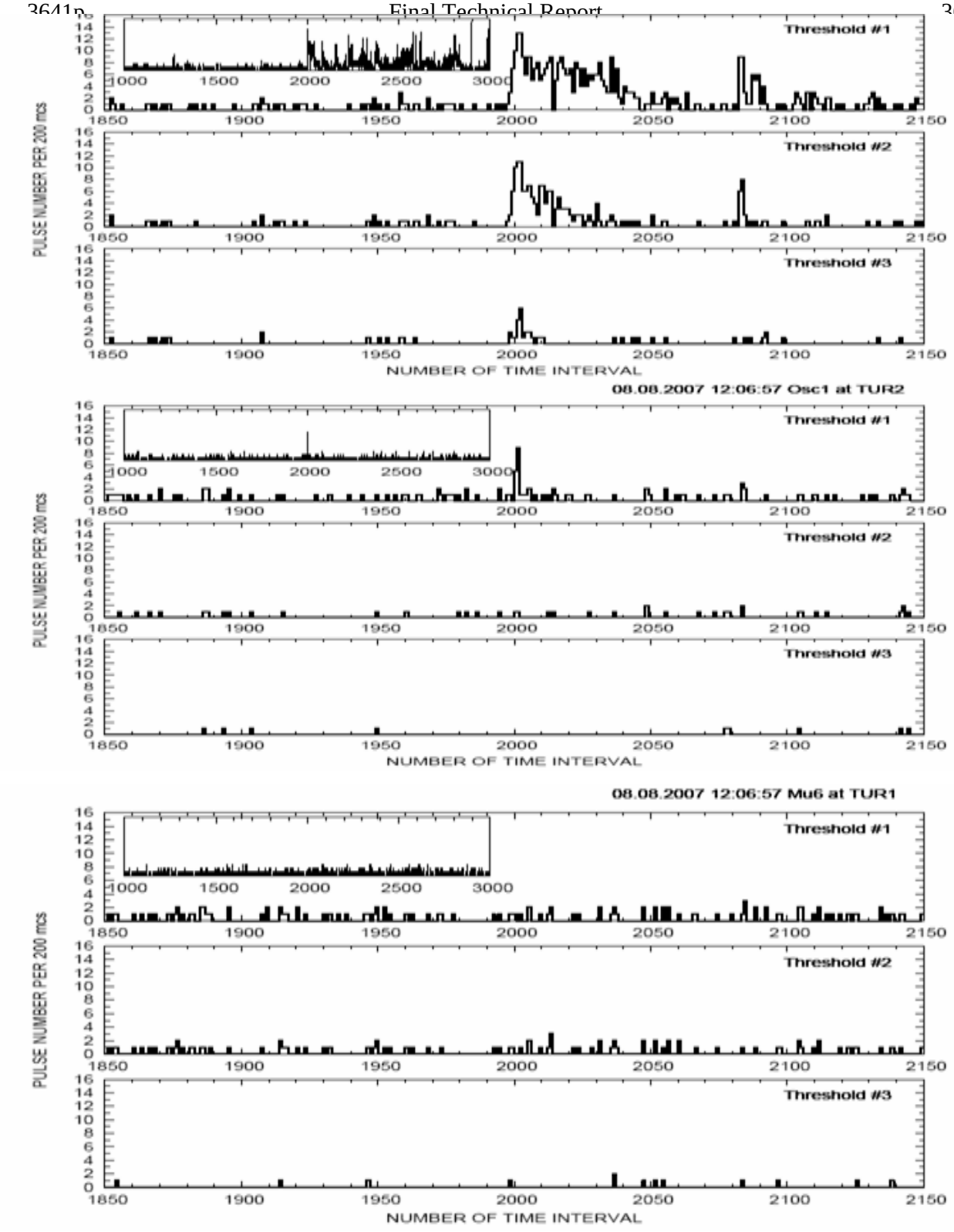

Fig.4.4. Gamma emission bursts registered by scintillate counters triggered by lightning. Intensities are shown for three registration points (TUR-III (540 m above the Tien-Shan Station level); TUR-II (310 m); KAPT (Tien-Shan Station level). The intensities for each counter are shown for three registration thresholds, which correspond to the minimum energy of registered quanta of 15, 60 and 240 keV.

Electron fluxes

During the 2009 thunder season on Tien-Shan Cosmic Ray Station the emission intensity was measured using the multi-layer absorption spectrometers bases on SI5G ionization counters. Unlike the measurements done in 1999-2004 the present ones were done using the system of time base which allowed microsecond resolution registering of the intensity change with time. The three-layer spectrometers in detector points *NEV* and *100M* were used.

The ionization counters SI5G were placed in each of the detector points in three layers ("up", "middle" and "lower") situated one above the other. Each layer consists of 60 counters. The sensitive area of each counter *(π x D x L)* is 0.11 m^2, the total sensitive area of one layer is about 6 m^2. Counters are situated in the wood boxes done out of the 5-mm thick plywood. A 30 mm thick rubber absorber separates the upper and middle layers while the middle and lower layers are separated with 1 mm lead sheet. The same sheet covers the floor of the detector point screening from below the whole detector assemblage from the base emission. The output signals of all counters of the same layer are bridged and are transferred to the registering system through the common cable.

Thus 3 signals are received by the data acquisition system from each of detector points *NEV* и *100M*. They are: pulses from upper, middle and lower layers of ionization counters.

Two additional signals, the coincidence (within 5 μs time gate) pulse between the counter layers ("upper" + "middle" and "upper" + "middle" + "lower") are formed in the data acquisition system itself. The efficiency of gamma quanta registration in SI5G counters is 0.05 - 2% depending on the energy while their efficiency of charged particle registering is about 95 - 99%. That's way the registering of the coincidence signals allows to distinguish the pulse from charged particles (electrons) from those from gamma quanta in the total pulse flow.

The data acquisition system allows obtaining the time scans of the intensity during 4000 serial time intervals having duration 200 μs each. The moment of the record of the scan is determined by a special signal – trigger which position in the time scan corresponds to the time interval having number 2000. Thus the time dependence of the intensity is represented during 2000 time intervals (0.4 s) before trigger moment and 2000 time intervals after this moment.

The trigger was formed in the same way as the electromagnetic trigger in 2007 year measurements. The trigger was formed as coincidence pulse of electromagnetic pulses induced on four long (500-1000 m) cables extended along the Station. At the end of the season (during thunderstorms on /08/30/09 and /09/01/09) the shower trigger system was used as well. It formed the trigger when the extensive atmosphere showers crossed simultaneously its six widespread detector points.

*The first type of registered even*ts (see for example Fig.4.5) is presented by time scans in wich short (having duration 1 -10 time intervals) growths of intensity in lower layer (some time even in middle) is seen while there was no any noticeable signal in the upper layer and no any coincidence signals. These events should be interpreted as the registration of the bremsstrahlung. The electrons accelerated in the thunderstorm electric field remain not registered in the upper cause the Compton effect and the photo effect in the absorber situated lower. The electrons arising in the process are registered by the counters situated in lower layers. At that the energy of gamma emission converts more effectively in the lead sheet determining the intensive signal from counters in the lower layer.

The cross section of photo effect rapidly decreases with the energy of electromagnetic emission. That's way the existence of such kind of events means that gamma quanta with energies up to 1 MeV are registered in the experiment. It corresponds to characteristic energies of bremsstrahlung from accelerated electrons and confirms our results of 2007 received by the use of NaI detectors.

Such type of events form the main part of registered events, they are observed exclusively in the active stage of a thunderstorm while they are completely missed during fine weather as well as during the rains and snowfalls (even intensive) without thunderstorms.

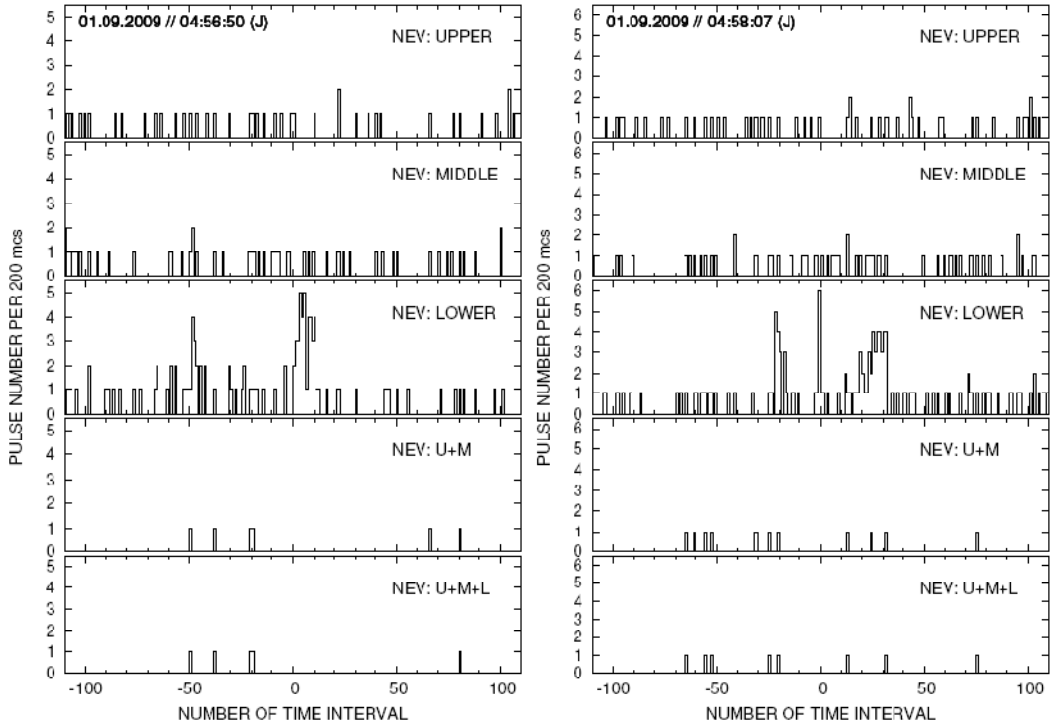
01.09.2009 // 04:56:50 (J)
NEV: UPPER
NEV: MIDDLE
NEV: LOWER
NEV: U+M
NEV: U+M+L
PULSE NUMBER PER 200 mcs
NUMBER OF TIME INTERVAL
01.09.2009 // 04:58:07 (J)
NEV: UPPER
NEV: MIDDLE
NEV: LOWER
NEV: U+M
NEV: U+M+L
PULSE NUMBER PER 200 mcs
NUMBER OF TIME INTERVAL

Fig.4.5

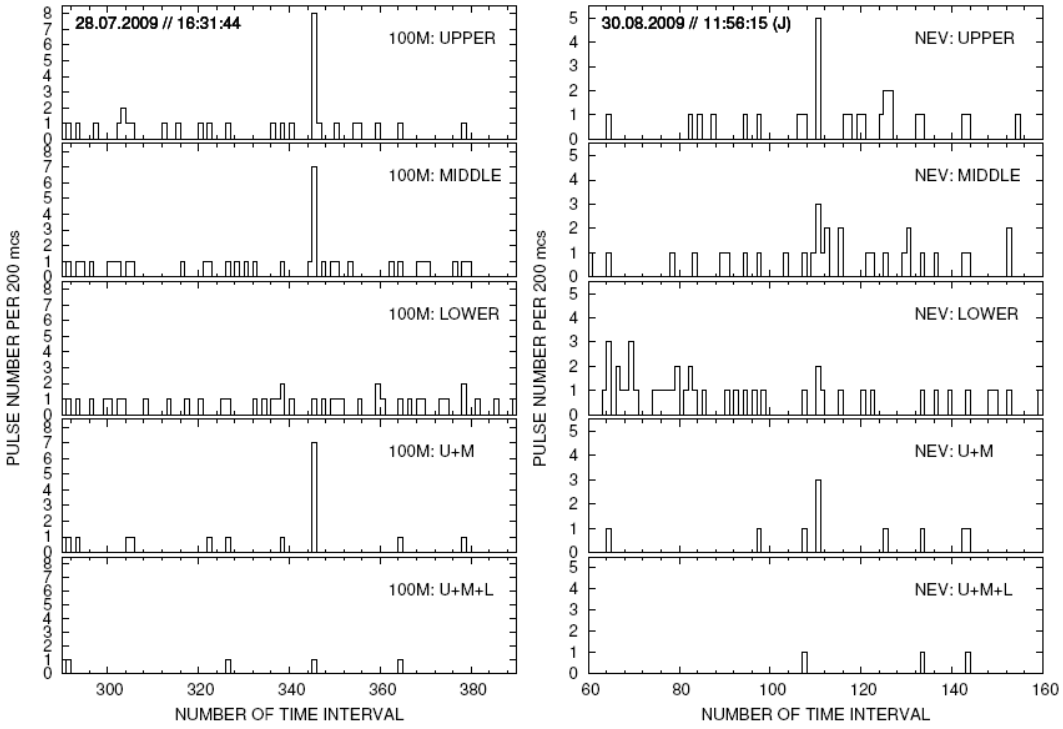
28.07.2009 // 16:31:44
100M: UPPER
100M: MIDDLE
100M: LOWER
100M: U+M
100M: U+M+L
PULSE NUMBER PER 200 mcs
NUMBER OF TIME INTERVAL
30.08.2009 // 11:56:15 (J)
NEV: UPPER
NEV: MIDDLE
NEV: LOWER
NEV: U+M
NEV: U+M+L
PULSE NUMBER PER 200 mcs
NUMBER OF TIME INTERVAL

Fig.4.6

The signals from electromagnetic emission are divided into two groups according to their durations: short flashes having duration 1-5 time intervals (i.e. less then 1 ms) and relatively long flashes having duration more then 10 time intervals, i.e. several microseconds. This distinction corresponds to that observed in 2007 in scans of gamma intensity measured by the use of NaI scintillators: short intensive flashes of gamma emission originated from the bremsstrahlung of electron avalanches and more long flashes of softer gamma emission registered usually in the events caused by the electromagnetic trigger.

Electromagnetic flashes overlap the moment of the trigger in about half part of all events. They come upon the time intervals with numbers ±10 - 20. It means that these flashes correspond to the moments of the maximum electric field strength which occur immediately before the lightning generating the trigger.

In *the second type* of events (see Fig.4.6) the narrow spikes of intensity (with characteristic duration – one time interval, i.e. 200 μs) are observed. These spikes simultaneously are displayed in the signals from upper, middle and lower layers of ionization counters as well as in the coincidence signals of both types. The probability to register series of quanta of electromagnetic radiation in two or even in three counter layers is negligible. Thus, the existence of coincidence signals means that these spikes correspond to cases of registration of electrons accelerated in the field of a thundercloud.

The events of registering of charged particles occur much often then the events with spikes in time scans. As opposite to the electromagnetic spikes scans with charged particles are observed only in one detector point. Thus, the characteristic path of electrons between these poins is about 150-160m. The events with charged particles just as events of the first type are observed exclusively in the active stage of a thunderstorm while they are completely missed during fine weather as well as during the rains and snowfalls (even intensive) without thunderstorms.

The base level of intensity for the coincidence signals is 0.07 - 0.1 pulses per one interval of the time scan. The typical number of coincidence signals is 3-5 pulses per interval, it for 30-70 times exceeds the base level. The placement of these signals on the time scale is rather uniform what confirms the year 2007 observations when narrow intensity spikes did not concentrate to the trigger moment also (in contradictory to the long flashes of soft emission with the events with electromagnetic trigger).

During the thunderstorm on September 1, 2009 both electromagnetic trigger and shower trigger were used. The last formed the trigger when the extensive atmosphere shower (EAS) passed through six detectors (*A, B, C, D, E, F*) widespread along the Station. The trigger was formed in the case of coincidence of at least four signals from detector points *A-F* within 2 μs time gate.

In some time scans of shower trigger events obtained during the thunderstorm on September 1, 2009 the intensive flashes of electromagnetic emission and the flows of charged particle correlated with these flashes. The flows of charged particle are observed nearby the moments of trigger left behind it for 1-2 time intervals. Most likely these intensive flashes are observed in the cases when the EAS direction was favorable and the flow of particles registered by the shower trigger system passed through the thundercloud. Events of such kind could be considered as a direct observation of the lightning initiation by the EAS particles.

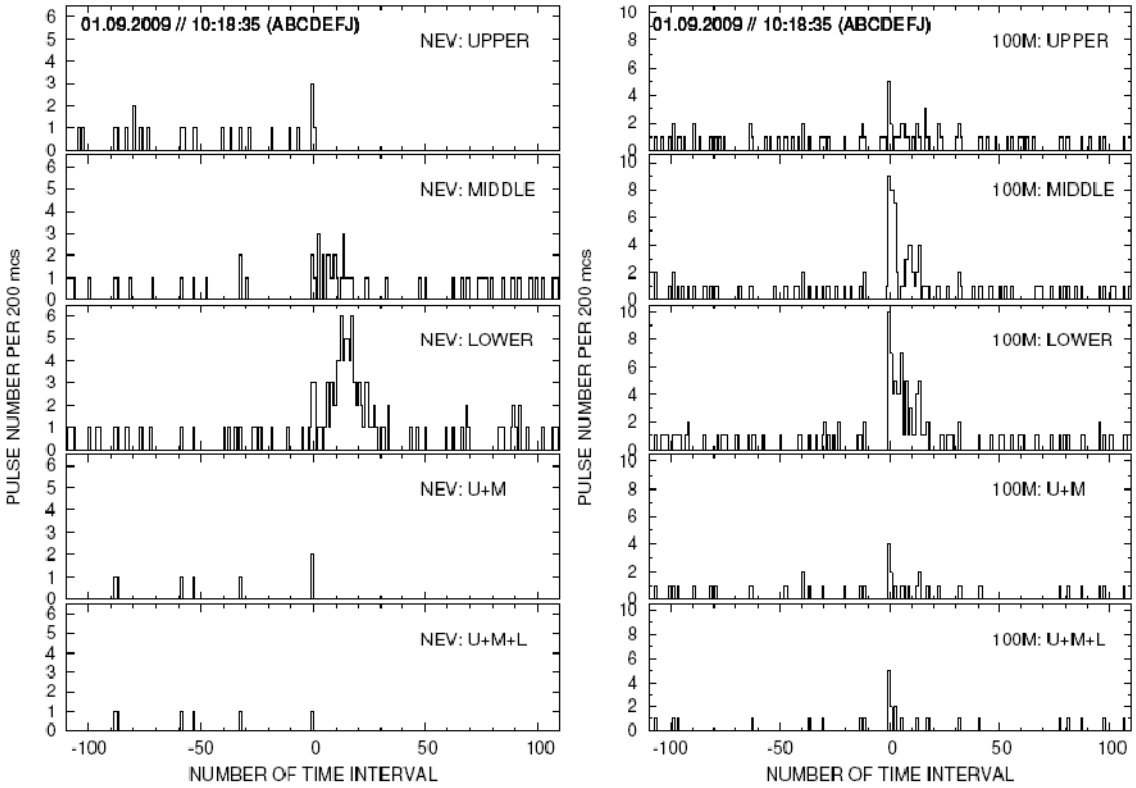

Fig.4.7

Theory

The theory of the lightning stepped leader which is under development in the Project conjointly takes into account three main processes: conventional breakdown, phenomenon of electron runaway and runaway breakdown.

STEPPED LEADER

The lightning leader steps have widely varied characteristics. According to the statements in the textbooks [1-2] based on the numerous measurements one can indicate the following main features of the steps.

(1) The step length is 3–50 m. As example one can take an average value 15 m. Note that the length is slightly growing with the atmospheric height.

(2) The step pulse duration is of the order 0.3–1 μs.

(3) The time between pulses either or between steps changes randomly from 5 to 100 μs.

(4) The pulse velocity obtained from the measurements of the luminosity movement is ~5×10^9 cm/s.

(5) The width of the luminous region is up to 1 m.

(6) The radio emission measured at the Earth surface demonstrate that the leader step pulse is accompanied by a significant pulse of electric current $I \sim 0.3–5$ kA.

CONVENTIONAL BREAKDOWN

Let us determine the basic pulse characteristics from the model of electric discharge in a strong electric field $E \sim 10E_{th} \approx 200$ kV/cm. The conventional breakdown in a given strong electric field leads to a very fast exponential growth of air ionization N_e

$$N_e = N_0 \exp(\nu_{ion} t) \qquad (1)$$

Here N_0 is the initial density of electrons and ν_{ion} is the ionization frequency. The breakdown in air was studied in details in numerous experimental and theoretical works (see textbooks [4-5]). The ionization frequency is growing effectively with the electric field value:

$$\nu_{ion} = \nu_{am} F(E / E_{th}). \tag{2}$$

Here ν_{am} is the maximal attachment frequency in e–O_2 collisions:

$$\nu_{ion} = 7.6\times10^{-13} N_m \ s^{-1} \approx 2\times10^{7}\left(\frac{N_m}{N_{m0}}\right) s^{-1}, \tag{3}$$

$$N_{m0} = 2.7\times10^{19} \ \text{cm}^{-3}$$

A well-known empirical formula [4] for F is

$$F = \left(E/E_{th}\right)^{5/3}. \tag{4}$$

It is correct at low values of E/Eth up to $E/E_{th} \sim 4$–5 (see [16]). At higher values of (E/E_{th}) the growth of νion/νam is diminishing reaching maximum $\sim 10^5$ approximately at $(E/E\text{th}) \approx 100$. In the region we are interested in

$$E/E_{th} = 7-10, \qquad \nu_{ion}/\nu_{am} = (2-5)\times10^{3} \tag{5}$$

So, we see from (1)–(5), that due to the breakdown in a given strong electric field the degree of ionization in air grows very rapidly.

On the other hand, the growth of the free electron density leads to the fast amplification of electron conductivity σ. The last process leads, as it is well known, to the diminishing of electric field:

$$E = E_0 \exp\left(-4\pi\int\sigma dt\right) \tag{6}$$

which will stop the growth of the ionization. Electrical conductivity in neutral atmosphere

$$\sigma = \frac{e^2 N_e}{m\nu_{em}}, \tag{7}$$

where ν_{em} is the electron collision frequency. Substituting (6), (7) in (1) we find that electric field keeps it's high value for the finite time $t < t^*$ when $N(t) \le N(t^*)$:

$$\frac{4\pi e^2 N(t^*)}{m\nu_{em}\nu_{am}F(E/E_{th})} \approx 1. \tag{8}$$

This relation determines the maximal value of electron density reaching in breakdown:

$$N_{em} = \frac{m\nu_{em}\nu_{am}}{4\pi e^2} F(E/E_{th}) \tag{9}$$

and characteristic time of the discharge

$$t^* = \frac{C_0}{\nu_{am}F(E/E_{th})}, \qquad C_0 \approx \ln\left(\frac{N_{em}}{N_e}\right) \approx 10-20. \tag{10}$$

Relations (9), (10) determine the basic characteristics of a strong electric field $(E>>E_{th})$ discharge in unbounded air

RUNAWAY ELECTRONS IN HIGH ELECTRIC FIELD

The electron runaway effect in gas under the action of the electric field is connected with the decreasing of the breaking force with the increasing of the electron energy ε:

$$F \approx \varepsilon\sigma_R N_a Z \propto \frac{1}{\varepsilon} \tag{11}$$

Here N_a – atomic number density, Z – charge of a nuclear, $\sigma_R \propto 1/\varepsilon^2$ – Rutherford cross-section. In the strong electric field E an electron of sufficient high energy

$$\varepsilon > \varepsilon_0 = \frac{eE}{\sigma_R Z N_a} \tag{12}$$

will be continuously accelerated. Such electrons are called runaway electrons. If the electric field is not too strong $E<<E_{cn}$ the main part of electrons having low energy $\varepsilon < \varepsilon_i$ (where ε_i is the ionization energy) are colliding with neutral atom as a whole. Friction force is

$$F = \sigma_a N_a \nu_T, \tag{13}$$

where m and ν_a electron mass and collision frequency

$$\nu_a = \sigma_a N_a \nu_T, \tag{14}$$

$\nu_T = \sqrt{T_e/m}$ —electron thermal velocity, σ_a—collision cross section. Eq. (13) determines usual drift of electrons under the action of electric field $E = F/e$. Thus we see that at low electron energies $\varepsilon < \varepsilon_i$ the friction force of electrons moving in the neutral gas F is growing with their energy. But at high energies $\varepsilon > \varepsilon_m$ it begins to fall down. It means that at some middle energies $\varepsilon \sim \varepsilon_m \sim Z\varepsilon_i$ it will reach the maximal value. We emphasize that around this region the interaction of fast electron with neutrals gradually transforms from elastic and inelastic scattering at the atom as a whole to the Coulomb scattering at the electrons and the atomic nucleus. To describe this process it is necessary to use the kinetic theory.

Kinetic theory of runaway electrons in neutral gasses was developed by Gurevich [6]. The electric field E was supposed homogeneous and the gas unbounded. According to the theory the maximal value of friction force F_{max} is characterized by the electric field E_{cn}:

$$E_{cn} = \frac{F_{\max}}{e} = \frac{4\pi e^3 N_a Z}{2.72 I}, \tag{15}$$

where I is an average excitation energy. Taking into account that $I \approx 13.5Z$ eV, an astonishingly simple expression for the value of critical field in neutral gas was obtained:

$$E_{cn} = 7\times10^{-15} N_a \text{ V/cm}. \tag{16}$$

Here N_a is the number density of atoms in cm^3. For example in air

$$E_{cn} = 38\left(\frac{N_m}{2.7\times10^{19}}\right) \text{ MV/m } \approx 20E_{th} \tag{17}$$

where N_m is the number density of air molecules, and E_{th}—a threshold electric field of conventional breakdown.

If the electric field is less than critical one $E < E_{cn}$ only the electrons in the tail of distribution function become runaways. The flux of runaway electrons is proportional to the exponential factor [6]:

$$S_r = \frac{dN}{dt} = N_e \nu_e \exp\left\{-\frac{E_{cn}}{2E} A\right\}. \tag{18}$$

Here N_e is the number density of electrons, ν_e—electron collision frequency at a characteristic runaway electron energy ε_c and A is a large constant (for air $A \approx 30$). It means that the number of runaway electrons falls down very rapidly with electric field decreasing. The basic theory was farther developed and confirmed for different gases in a number theoretical and experimental studies (see textbooks [7,8]).

RUNAWAY BREAKDOWN IN STRONG ELECTRIC FIELD

The basic physical process determining the phenomenon of runaway breakdown (RB) is the generation of new fast electrons due to the runaway particle ionization of neutral molecules.

Although the majority of newborn free electrons have low energies, some will have rather high energy $\varepsilon > \varepsilon_c$. As a result, an exponentially growing runaway avalanche can occur. Two main features of RB are:

(1) It can occur in the electric field $E > E_c$, where E_c is an order of magnitude less then the threshold field of conventional breakdown $E_c << E_{th}$.

(2) The presence of "seed" fast electrons having energies above the critical runaway energy ε_c is needed to initiate RB.

In the previous works the RB theory in weak electric fields $E << E_{th}$ was constructed and a role of RB in lightning leader initiation was studied [10-11]. But one can show that the runaway breakdown effect can take place in a strong electric field $E >> E_{th}$ as well. Our goal is to develop such a theory – the theory of strong runaway breakdown (SRB). It will be shown that usual runaway electrons serve as a seed for SRB, when their energy reach the runaway critical energy ε_c which coincide exactly with the one determined in the weak RB theory: $\varepsilon_c = (mc^2/2)(E_c/E)$. Thus the usual runaway effect in neutral gases gradually transforms to SRB, at electron energies ε:

$$\varepsilon \geq \varepsilon_c = (mc^2/2)(E_c/E) \approx 25\left(E_{th}/E\right) \text{ keV} \qquad (19)$$

Here we took into account that for air $E_c/E_{th} \approx 0.1$. It is evident from (17) and (18) that SRB effect at $E \sim (1\text{-}4)E_{th}$ is extremely low. It explains that in usual long sparks $E \leq (3\text{-}4)\, E_{th}$ (see [12]) the runaway electrons and gamma emission are practically absent. On the contrary, at $E/E_{th} \geq$ 7-10 the runaways could become significant what lead to the exponentially strong SRB.

Temporal and spatial growth of runaway breakdown in strong electric field

Let us consider the strong runaway breakdown (SRB) effect in a strong electric field $E/E_{th} \approx 7$–10. It means that parameter $\delta = E/E_c \approx 70$–100. In such strong fields we can consider the main part of distribution function in nonrelativistic limit. Moreover, the distribution function is directional along electric field. The kinetic equation describing runaway breakdown in this case has a form [13]

$$\frac{\partial f}{\partial t} + v\frac{\partial f}{\partial z} + \delta\frac{1}{v^2}\left(v^2 f\right) = \frac{1}{v^2}\frac{\partial f}{\partial v} + \frac{1}{\Lambda v^5}\int_v^\infty f(k)kdk. \qquad (20)$$

Here z—direction along electric field, Λ—Bethe's logarithm. Eq. (20) has a very important feature: the parameter δ could be eliminated from equation. Actually, introducing

$$F = \int_\infty^u f(k)kdk, \qquad (21)$$

$$x = z\delta^2, \qquad \tau = t\delta^{3/2}, \qquad u = v\delta^{1/2} \qquad (22)$$

we can rewrite Eq. (20) in the form

$$\frac{\partial^2 F}{\partial v \partial x} + \frac{1}{u}\frac{\partial^2 F}{\partial u \partial \tau} + \frac{1}{u^2}\frac{\partial}{\partial u}\left(\frac{1}{u}\frac{\partial F}{\partial u}\right) - \frac{F}{\Lambda u^5}. \qquad (23)$$

This self-similarity of Eq. (23) on parameter δ means that we can solve it for $\delta = 1$ and automatically find from (22) the runaway breakdown growth rates for arbitrary δ.

Let us consider first the limit case of spatial uniform time growth.

In this case we can search for the solution of Eq. (20) in the form $f(v, t) = f(v) \exp(t/\tau_{rb})$. According to (21), (23) the time of exponential growth of electrons

$$\tau_{rb} = \tau_0 \delta^{-3/2}. \qquad (24)$$

This result is in agreement with spatially uniform runaway breakdown theory [13].

(2) Spatial dependence

In this case we can search for the solution of Eq. (20) in the form $f(v, t) = f(v) \exp(z/la)$. According to (21), (23) the avalanche scale l_a decrease with increasing δ

$$l_a = l_0 \delta^{-2} \qquad (25).$$

It means that the avalanche length in a strong field is diminishing dramatically. Thus, in air for $\delta = 70–100$ we have $l_a \approx 1$ cm. The distribution function for $\delta = 70$ and the growth of runaway electron density for $\delta = 70, 100$ determined by numerical solution of Eq. (23) are presented at Figs. 4.8, 4.9. The results are in agreement with studied previously runaway breakdown for the case of a weak electric field. The distribution function is approaching rapidly to $f \sim 1/\varepsilon$. The characteristic time-scale of SRB process in atmosphere is of the order of a few ns. Note that the density growth is stronger during the initial 0.5 ns, analogous effect was seen in the weak fields (see [13]).

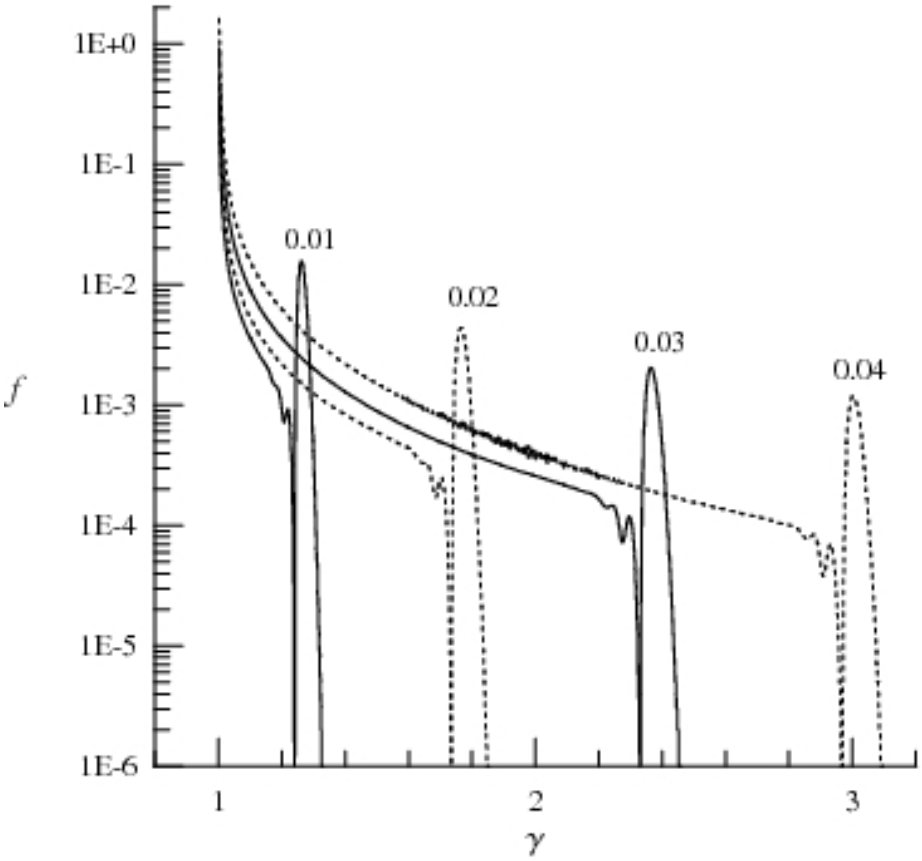

Fig.4.8. Dependence of distribution function of fast electrons on energy for $\delta = 100$. Different curves correspond to time moments 0.01, 0.02, 0.03 and 0.04. Asymptotic behavior $f \sim 1/\varepsilon$ is clearly seen.

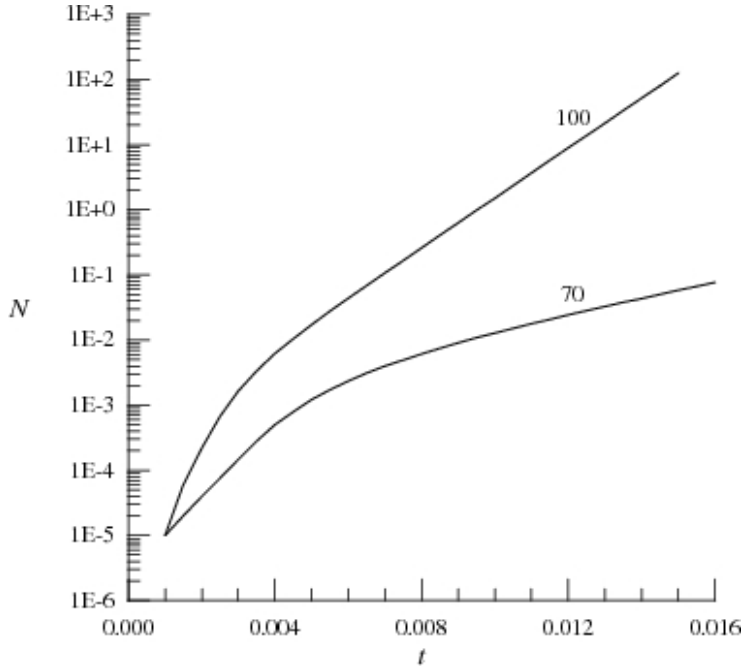

Fig.4.9. Growth of total number of fast electrons with time for parameters $\delta = 100$ and $\delta = 70$.

References

1. M.A. Uman, The Lightning Discharge, Academic Press, New York, 2001.
2. D.M. Gorman, W.D. Rust, The Electric Nature of Storms, Oxford Univ.Press, New York, 1998.
3. A.D. Mac-Donald, Microwave Breakdown in Gases, Wiley, New York, 1965.
4. A.V. Gurevich, N.D. Borisov, G.M. Milikh, Physics of Microwave Discharges, Gordon & Breach, New York, 2000
5. H.A. Bethe, Ann. Phys. (Leipzig) 5 (1930) 325.
6. A.V. Gurevich, ЖЭТФ 39 (1960) 1296, Sov. Phys. JETP 12 (1961) 904.
7. Yu.N. Dnestrovskii, D.P. Kostomarov, Mathematical Simulations in Plasma, Nauka, Moscow, 1991.
8. Yu.D. Korolev, G.A. Mesyats, Physics of Pulse Breakdown in Gases, Nauka, Moscow, 1991.
9. A.V. Gurevich, G.M. Milikh, R.A. Roussel-Dupre, Phys. Lett. A 165 (1992) 463.
10. A.V. Gurevich, Yu.V. Medvedev, K.P. Zybin, Phys. Lett. A 329 (2004) 348.
11. A.V. Gurevich, K.P. Zybin, Yu.V. Medvedev, Phys. Lett. A 349 (2006) 331.
12. E.M. Bazlyan, Yu.P. Raizer, Lightning Physics and Lightning Protection.
13. A.V. Gurevich, K.P. Zybin, Phys. Today (May 2005) 37;
    A.V. Gurevich, K.P. Zybin, Phys. Usp. 44 (2001) 1119.

Numerical simulations of runaway breakdown in inhomogeneous medium

The electron generation during runaway breakdown in the case of spatial non-uniformity was studied. The computations are performed by means of the program for solving the kinetic equation that takes into account the dependence of the electron distribution function on coordinate. It is found that the electron density increases sharply near the point where the electric field is maximal. The region of the electron density increasing is small enough. Here the flow velocity of electrons is abruptly increasing. The spatial distributions of the electron density and flow velocity are illustrated in Fig.4.10. The distributions are given at time t=0.05 (dashed and dot-dashed curves, respectively) and t=0.1 (solid and dotted curves, respectively). The electric field amplitude E/E_0=50.

Numerical computations show that the initial electron flow velocity has a small effect on the rate of the electron generation. The effect depends on the electric field amplitude. Also, there is a small effect of the size of the electric field region.

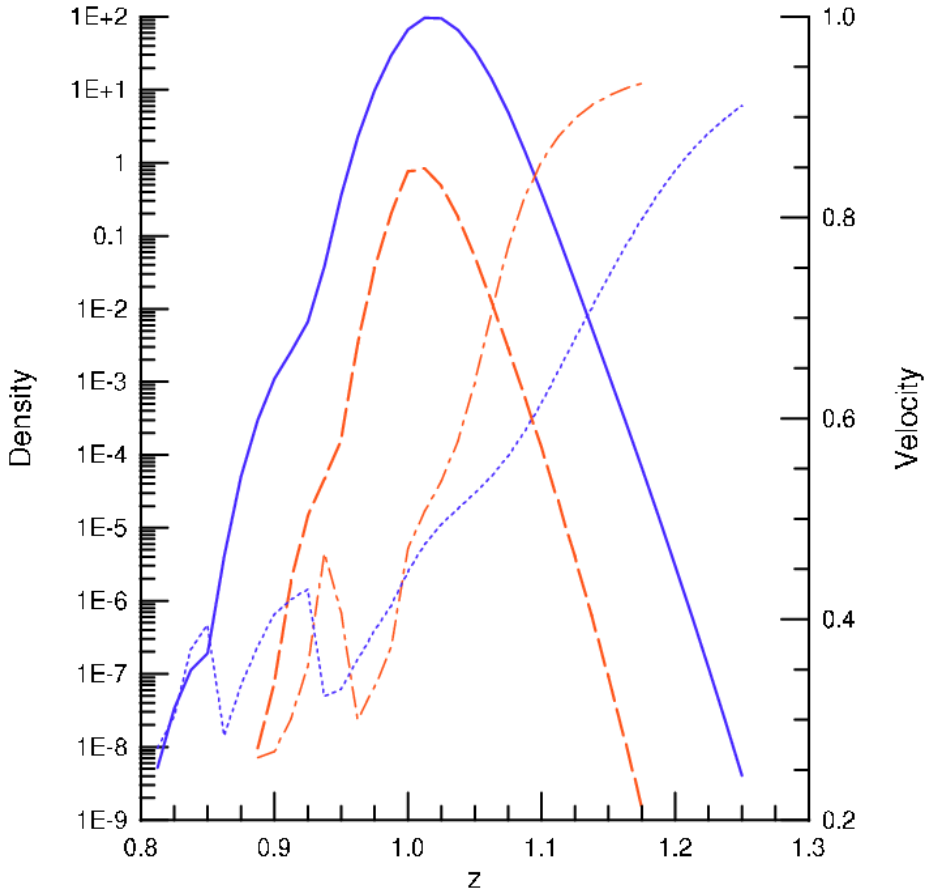

Fig.4.10. Spatial distributions of the electron density and flow velocity

The numerical investigation of the runaway breakdown on the front of the relativistic wave was studied. The increment of the particle number increasing strongly increase with the increasing of the electric field amplitude E/E_0, where E_0 – the critical field of breakdown. It is clearly seen in Fig 4.11 were the time dependences of the electron density are presented for different values of E/E_0. Since the time t=0.01 electron density exponentially increases with the constant increment. Its value is in a good agreement with the theoretically expected dependence $0.35\ (E/E_0)^{3/2}$. The deviations to the more small values are observed at relatively small values of $E/E_0 \leq 15$. Electrons with small energies $\gamma \leq 3$ give the main contribution into the density.

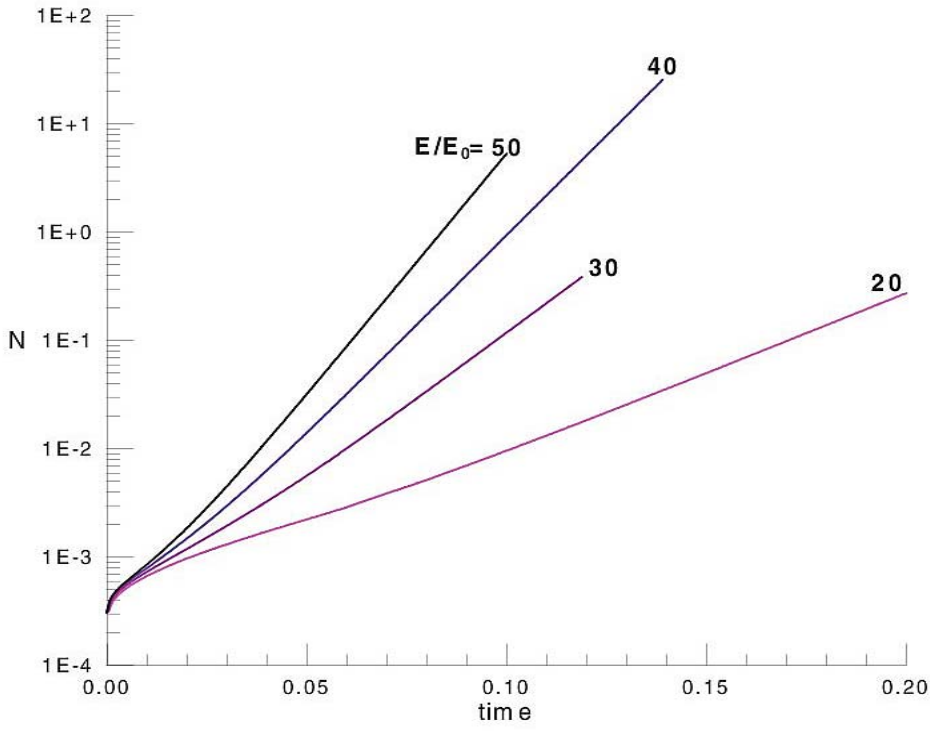

Fig.4.11. Growth of fast electron number as a function of the electric field amplitude.

Task 5: Transformation of an extensive atmospheric shower in the thunder electric field: intensive growth of electromagnetic component, namely of the high-energy electrons number, of gamma quanta and positrons number. Space enlargement of the shower. Experimental and theoretical investigation

Experiment

During a summer season thunderstorm clouds pass directly at the height of the Station (3340 above see level), so the installation detectors are located deeply inside of a cloud. In the summer season 2007Y the on-line monitoring of extensive air showers was carried out and their correlations with flares of gamma and X-radiation were studied. The goal of the investigations was to check theoretical predictions of combined effects of runaway breakdown and high-energy cosmic rays ($E \geq 10^{15}$–10^{16} eV) on lightning processes in the thunderstorm atmosphere.

The measurements with scintillation NaI-detectors included registration of the intensity in slow and fast (100-200 μs) time span. Measurements with the high resolution were conducted in 4000 consecutive time slots having 200 μs duration; 2000 intervals before and 2000 after the trigger moment. The measurements were carried out using the system of NaI-detectors with the wide site separation (~2 km in a horizontal and ~500-600 m in a vertical direction). Short flares of radiations were found for the first time in measurements with the high temporary resolutions. They have complex structure indicating the presence of electrons accelerated till 10-30 MeV as well as electrons having low (tens keV) and high (deciles and units of MeV) energies.

Three types of trigger signals were used in measurements with the high resolution: the EAS trigger, "jump of a field" trigger and electromagnetic pulse trigger. Four separate systems of concurrences constructed on the base hodoscopes from SI5G Geiger counters were used for a trigger pulse creation at the moment of EAS passage through the installation. The EAS trigger pulse initiated the data recording from all subsystems of a "THUNDERSTORM" complex.

The lightning discharge electromagnetic emission was studied using two radio installations in the 0.1–30 MHz frequency range. They allowed registering the pulse waveform with 16 ns time accuracy as well as to determine the direction of the emission source. The installation "*Radio-E"* was used in the measurements as well. The operation threshold was chosen too large in the 2007 season, thus it corresponded to the nearby discharges only. That why the total number of the produced drive pulses was small compared to the previous seasons when the threshold was noticeably lower and false events where registered due to the noise even without thunderstorm. Radio installations "Radio-HF" were set going by the trigger pulses from the "Radio-E" installation as well as from the *storm trigger system*. Moreover, installations could be set going spontaneously due to the interference induction from the lightning discharges, most likely on the flux, – electromagnetic pulses (EMP). It could be supposed that at least in some cases these are the same pulses that set going the scintillate detector record system. It must be mentioned that not all of the trigger pulses could be processed by the radio installations. It concerns with the large data amount obtained in the single event. Data must be recorded of the hard disk of the computer, the record of one event takes 30 seconds, at that the record time varies from one vent to the other and varies for different installations. The trigger pulses coming during the recording are not processed. The comparison of data obtained in simultaneous measurements of gamma and radio emission showed that as a rule both emissions are observed in those cases when it could be supposed that the startup of corresponding installations takes place due to the same EMP. A record example with the assumption of the synchronous operating time of installations is shown in Fig.5.1.

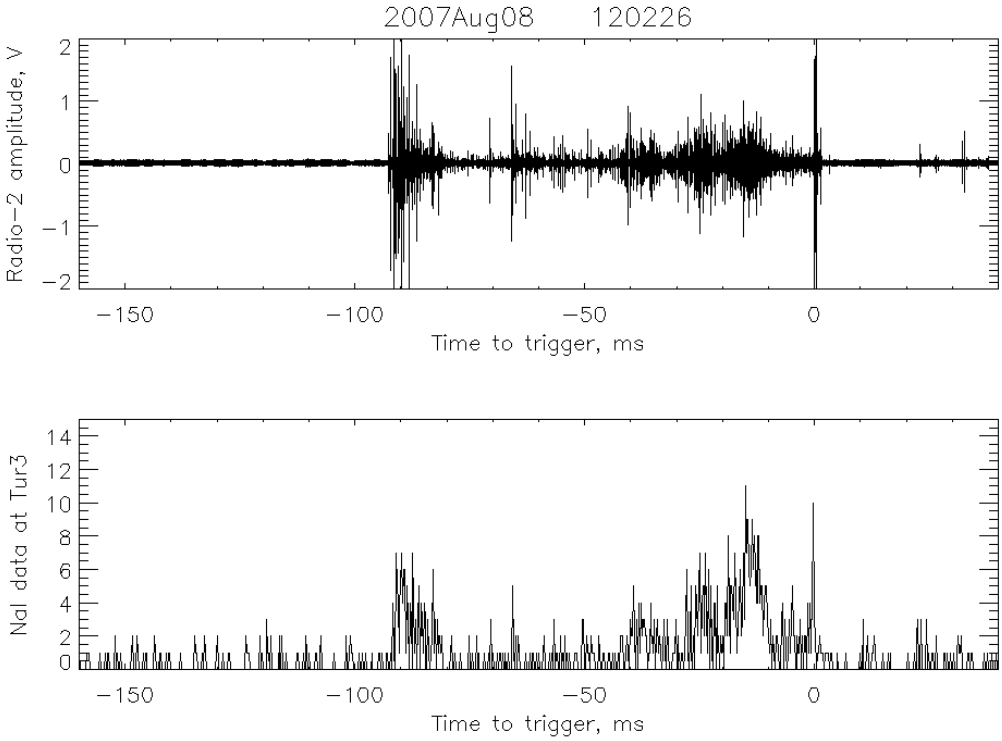

Fig. 5.1.

The high time correlation between gamma and radio emission is seen in the event. In Fig.5.2 quasi-stationary electric field in the same time range is shown. The minor field jump is observed corresponding to the distant cloud-to ground discharge. It should be mentioned that the time lock-on of the data obtained on the “Radio-E” installation to the other installations could be done in 2007 campaign with not best than the second accuracy.

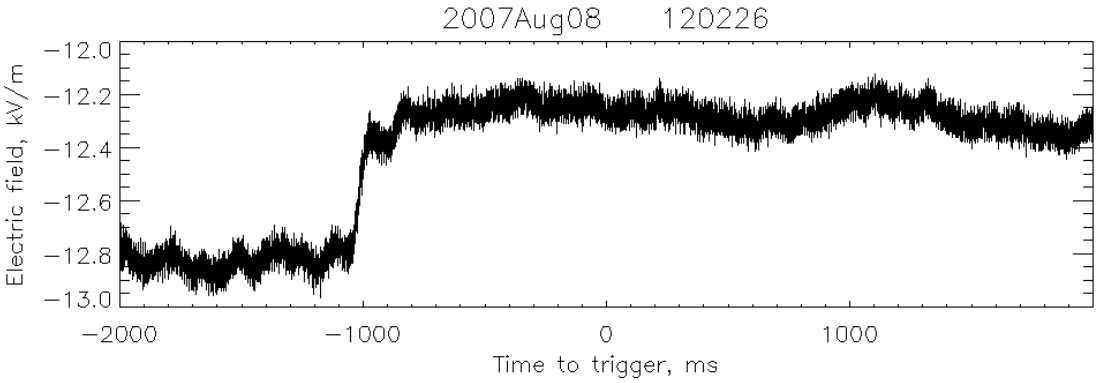

Fig. 5.2.

Gamma and radio emission is observed in events corresponding to the EAS trigger rarely than in the events corresponding to the EMP trigger, radio emission is observed more often than gamma one. It is determined by the fact that the passage of the shower is not specially or temporally connected with the existence of strong electric field in the thundercloud, typical for the lightning discharge initiation. According to that most showers on the one hand can’t initiate the runaway breakdown effect in a cloud and on the other hand can’t be affected by the thunder electric field. In the opposite case, when the shower passes through the strong electric field region of the thundercloud which exceeds the threshold electric field of runaway breakdown, the EAS could be the initiator of the lightning discharge generating powerful E-field and gamma emissions. It could be observed at that if sensors are not far from the region where EAS interacts with the cloud, due to the small gamma ray path length in atmosphere. In opposite, the radio emission could be observed from the large distance from the interaction region. An example of the probable lightning initiation by the EAS is shown in Fig. 5.3, the discharge beginning coincides in time with the shower passage. The gamma emission in this event was not observed, most likely due to its remoteness from the sensor placement. An example of event corresponding to the EAS trigger is shown in Fig.5.4. Both radio and gamma emission are observed, they are well correlated. It should be mentioned that in this event the registered shower did not initiate the lightning discharge, the emission started earlier, but it have through the region of the strong electric field where the discharge was developed. It appeared in the existence of intensive pulse of gamma and radio emission at the moment corresponding to the shower passage time.

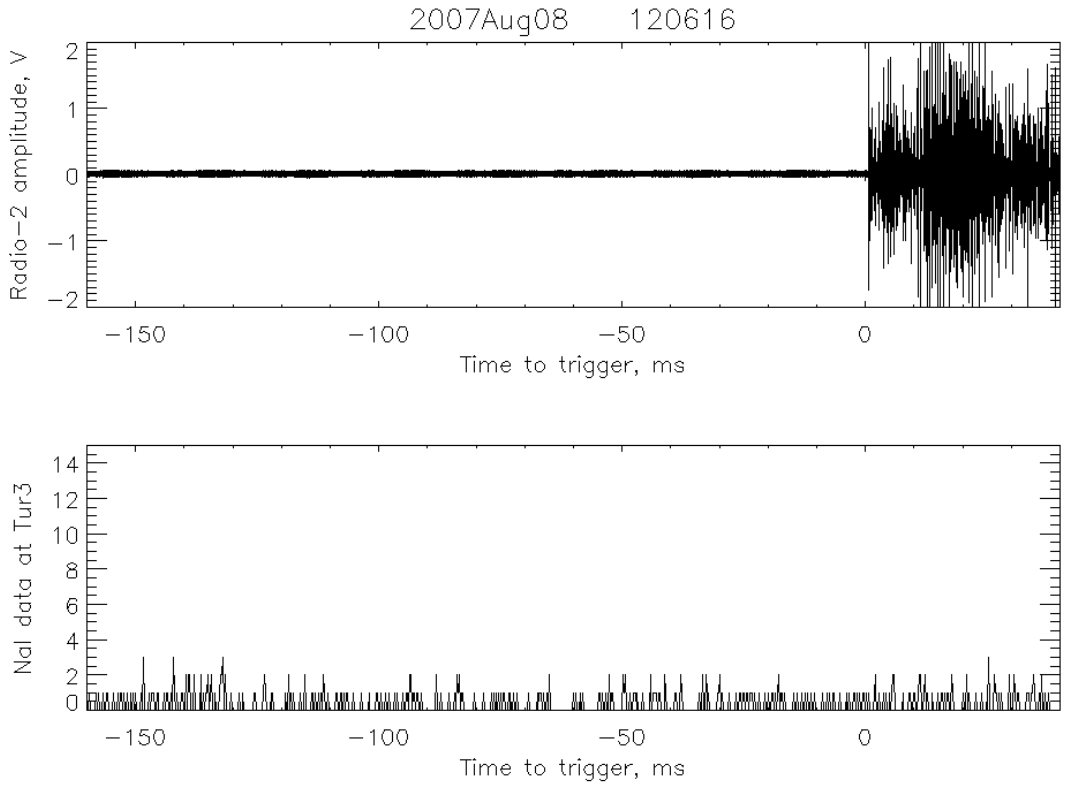
2007Aug08 120616
Radio−2 amplitude, V
2
1
0
−1
−2
−150
−100
−50
0
Time to trigger, ms
NaI data at Tur3
14
12
10
8
6
4
2
0
−150
−100
−50
0
Time to trigger, ms

Fig.5.3.

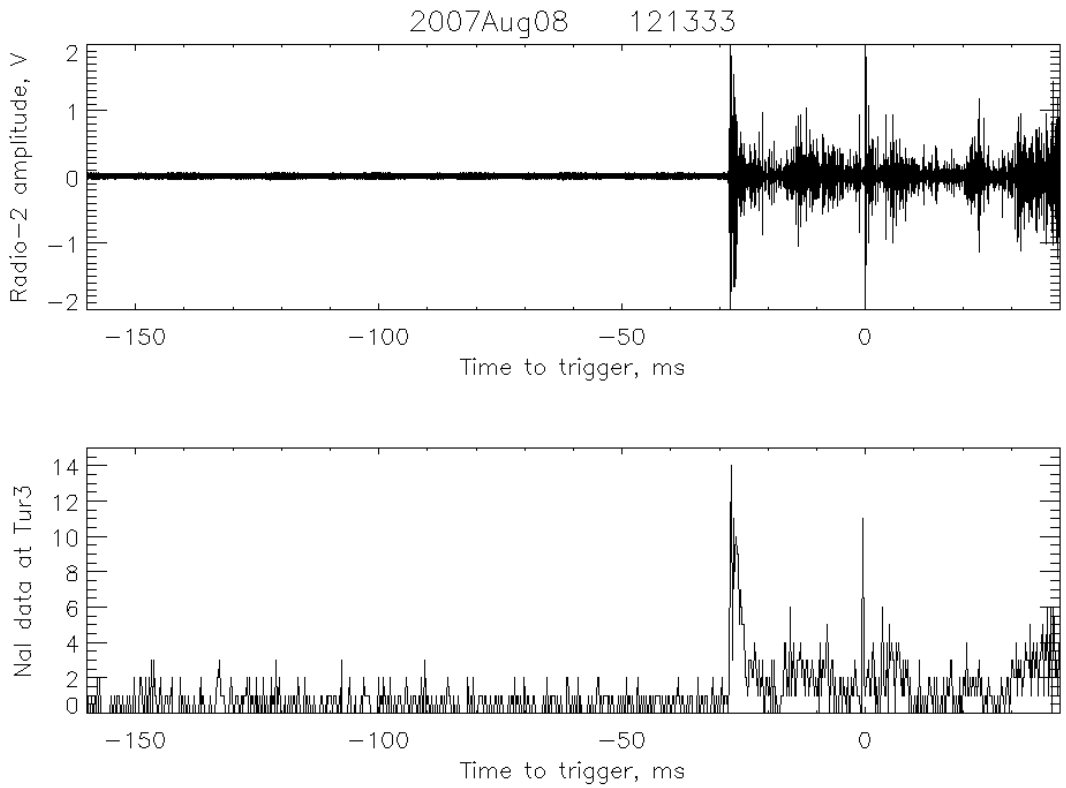
2007Aug08 121333
Radio−2 amplitude, V
2
1
0
−1
−2
−150
−100
−50
0
Time to trigger, ms
NaI data at Tur3
14
12
10
8
6
4
2
0
−150
−100
−50
0
Time to trigger, ms

Fig.5.4.

The system of gamma-radiation detectors permits to analyze the amplitude information of the input scintillation signals. To use this information the absolute detector calibration is needed. A connection between the six thresholds of pulse discriminators of the registration system, and corresponding ranges of energy deposit of gamma-radiation quanta inside the scintillating crystal was determined. After calibration it was established that pulse discriminators have monotonously increasing operation thresholds, corresponding to gamma-quanta energy range: 30, 40, 60, 70, 120 and 320 keV.

The spatial distribution of bursts observed in our experiment is about 1 km as it is seen simultaneously at four detector points for all energy thresholds. We have compared the data for different energy thresholds at different detector points and found that the integral energy spectrum is similar. It allowed us to construct the averaged integral spectrum taking into account the results of detector calibration. The spectrum is presented at the Fig.5.5. It demonstrates a good agreement of our experiments both with the Eack et al. balloon experiments [5] and with runaway breakdown theory.

.

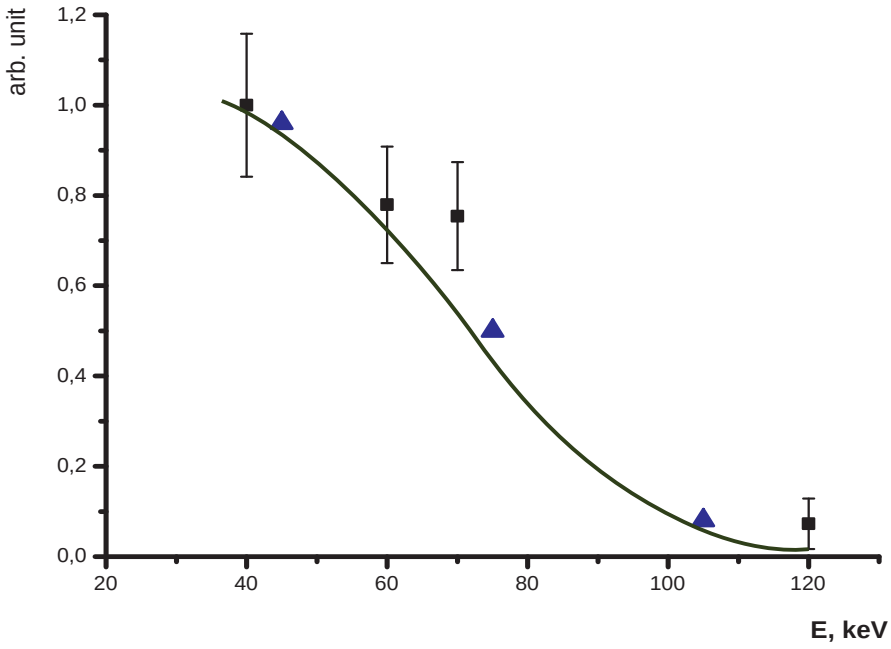

Figure 5.5. Integral energy spectrum of short-time gamma flashes in the thunderstorm atmosphere: data of Tien-Shan experimental (squares), theoretical curve (solid line) and balloon experiment data by Eack et al. [5] (triangles).

The EAS triggered gamma bursts were studied. The typical example of such an event is presented at Fig 5.1. The burst of gamma emission of the type as in Fig 5.6 time scans lasts for about one millisecond. This burst is the powerful single outburst of hard gamma quanta registered in all three energy diapasons. Besides, time scans in Fig 5.6 demonstrate the wide space distribution of the emission of the burst. The signal is observed in registration points TUR3, TUR2 and KAPT without significant depression. It disappears only in lower point NEV.

The probability to observe the EAS triggered burst in the time scan increases from 2 % in fair weather to 10% when thundercloud do exist. The total fraction of bursts registered in time scans is quit a few (only 10% even in the thunder case) among all registered EAS. It could be apparently explained by the relatively small area of the shower trigger system used in the

experiment and its large distance from those registering points where the most powerful signals from bursts were observed, i.e. from “upper” scintillators TUR3, TUR2 and TUR1.

The temporary correlation of short-term flares with the moments of EAS passage through area with high intensity of an electrical field inside clouds is found. The flashes observable at the EAS trigger have much smaller duration (parts of ms) compared to the case of the electromagnetic trigger and are formed by gammas with ~ MeV energy. Spatial area of these flashes is much more wide ~ 1-2 km.

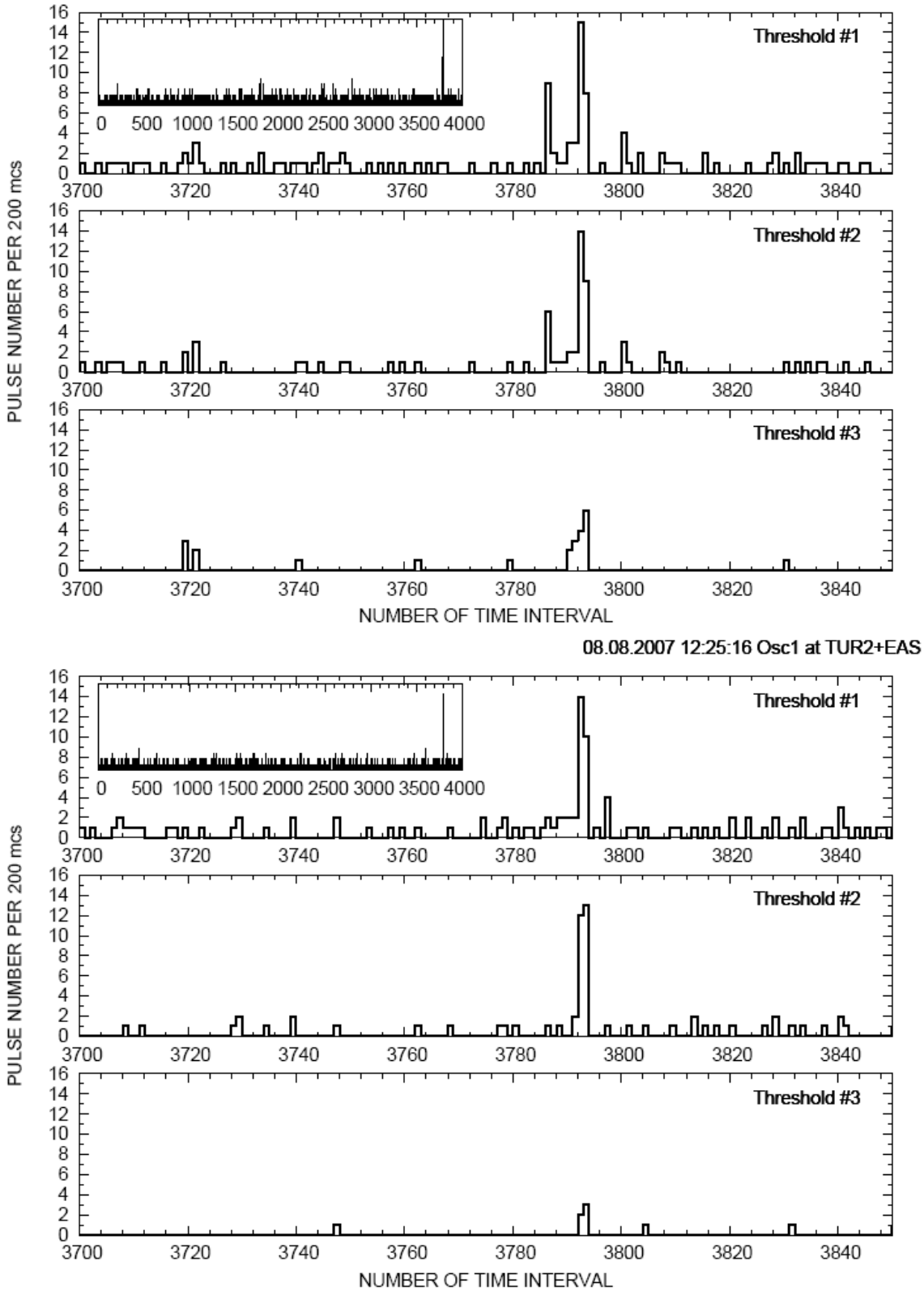

Fig.5.6. EAS triggered event: time scans of the gamma emission intensity at the height 540 m (TUR3) and 310 m ({TUR2) above the average level of the Tien-Shan Station. Abscissa axis: the number of the time interval, 200 μs each.

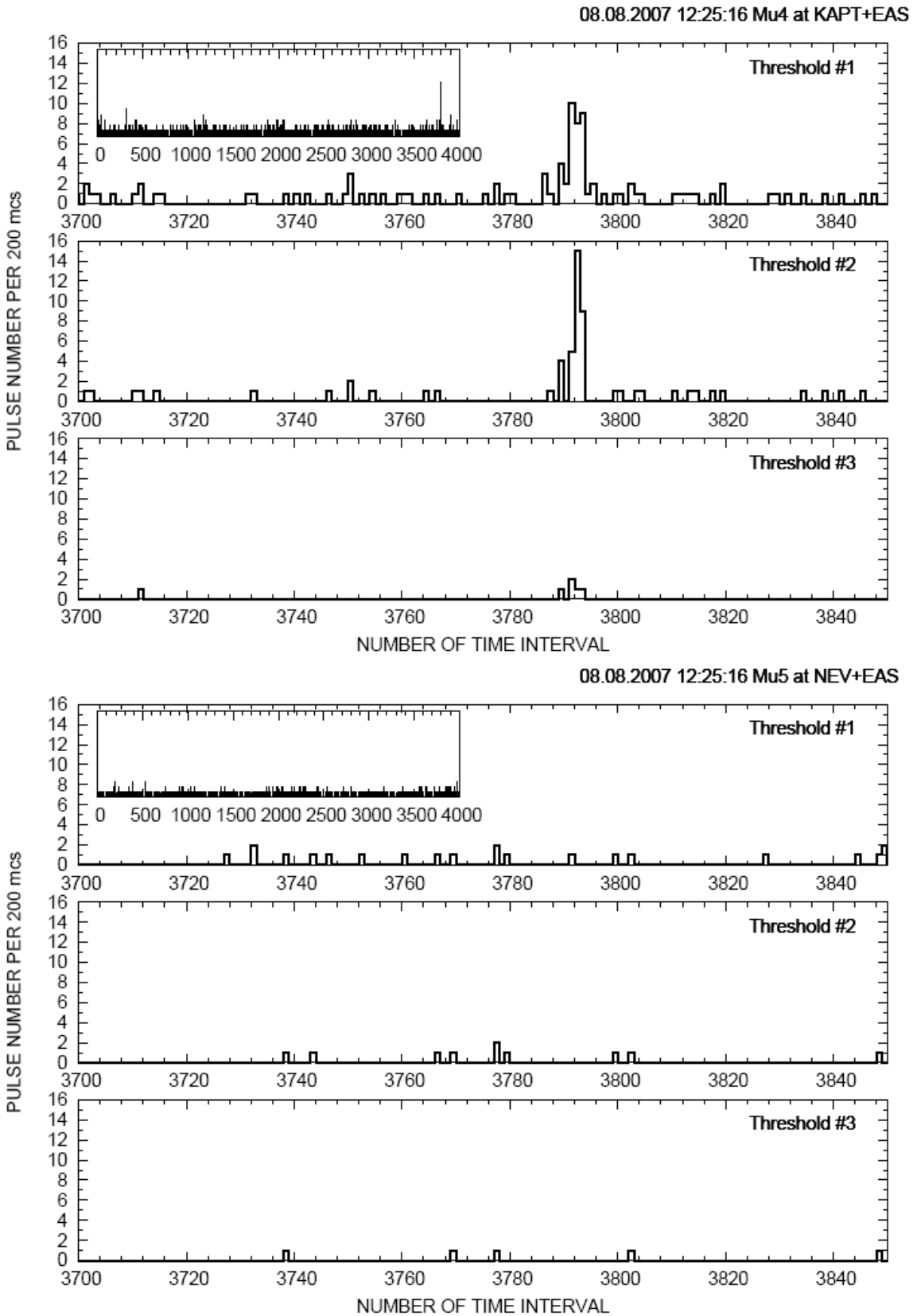

Рис.5.6. (Continued). EAS triggered event: time scans of the gamma emission intensity at the height 60 m (KAPT) and at the Tien-Shan Station level (NEV).

During 11 hours of thunderstorm in August, 2007 we observed 600 events triggered by EAS. Strongly amplified pulse of gamma radiation simultaneously with EAS was seen in 4 events. One event happened 15.08.07 during initial phase of thunderstorm, other three events took place 08.08.07 during the main phase of the storm. Two events will describe here: one in the initial, another one in the main phase.

Event 15.08.07

Storm lasted 15.08.07 for four hours from 05.18 up to 09.40. The event took place at 05:18:12 in the initial phase of the storm. The shower was fixed by all six detectors of EAS trigger system. That means the EAS was generated by cosmic ray particle with the energy not less than 10^{16} eV. The pulse of gamma emission was seen at the scans of three observational points: 7, 6 and 4. The scans are presented in the Fig.5.7.

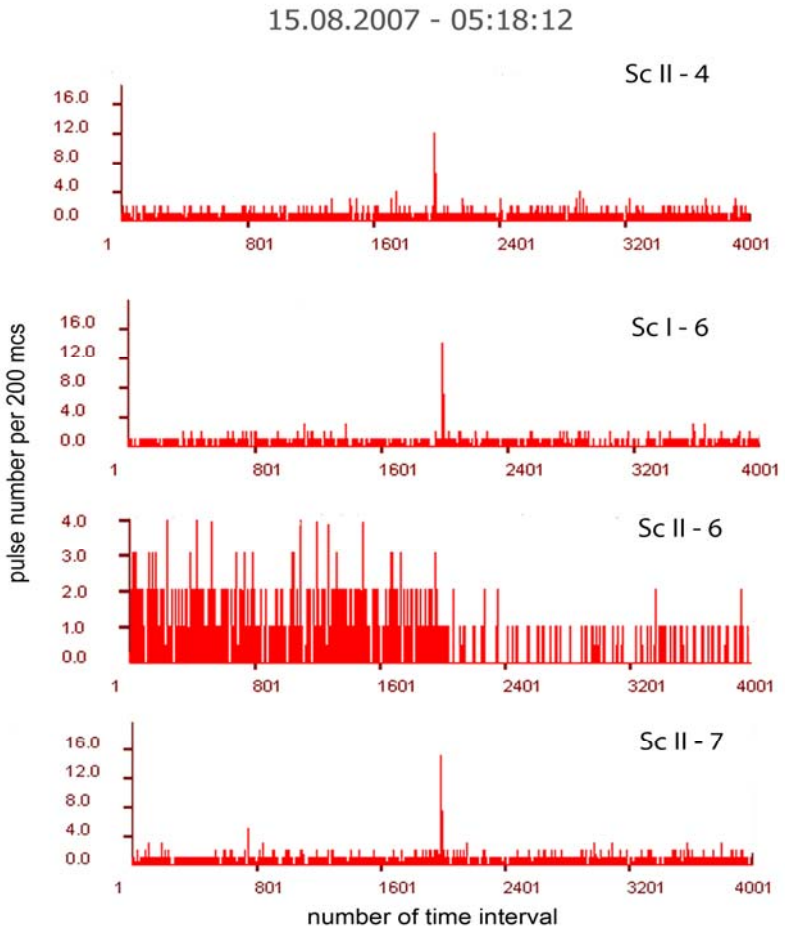

Fig.5.7. Time scans of gamma emission for the event 15.08.07. Each time interval is equal to 200 mcs. The moment of the EAS trigger corresponds to 2000-th time interval.

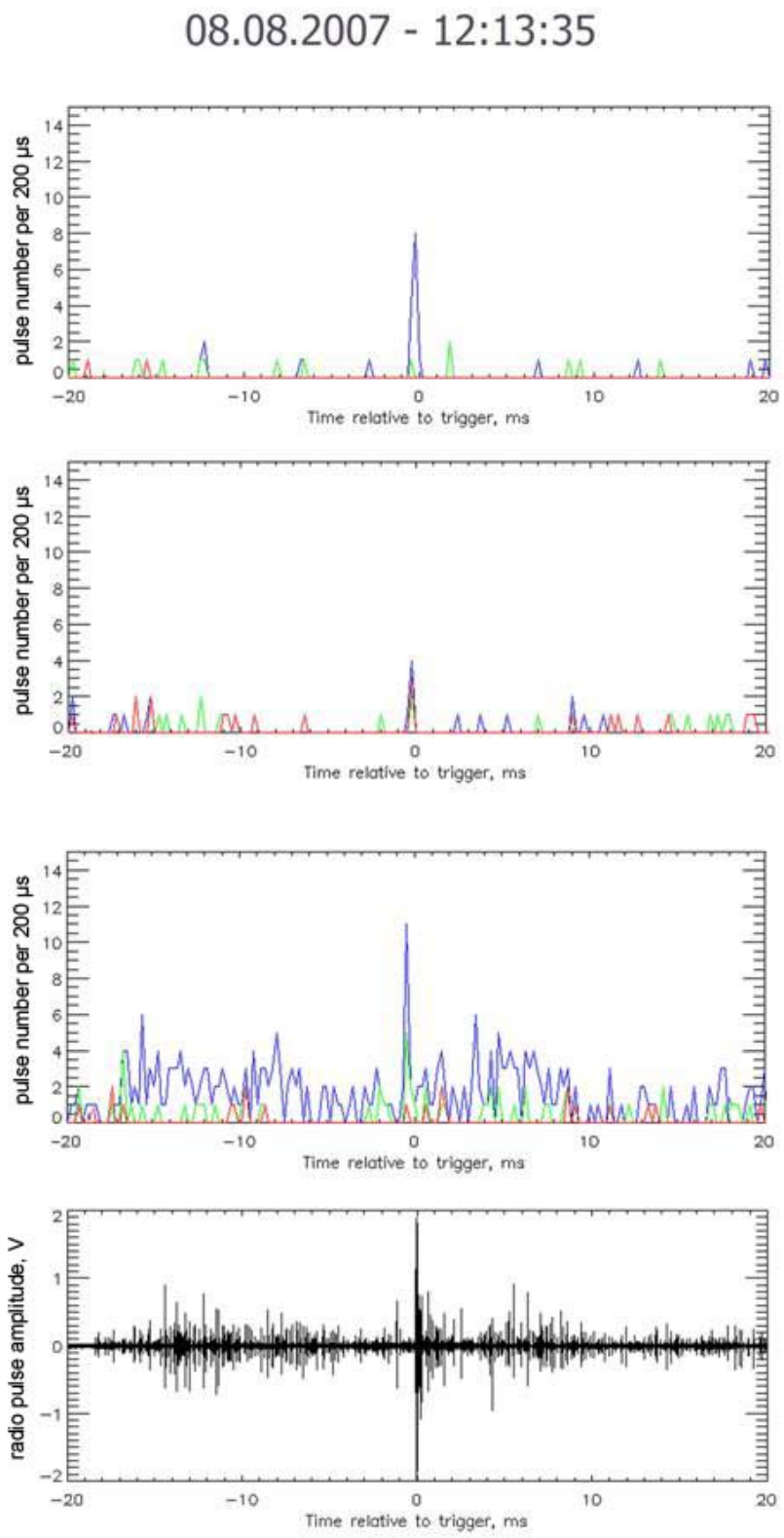

Fig. 5.8. Time scans for the event 08.08.07. From up to down: gamma emission measured by detectors ScI-5, ScI-6 and ScII-7. The bottom scan: HF radio emission.
The zero is the moment of the EAS trigger.

One can see from the Fig. 5.7:

- The strong pulse of gamma emission was observed in all points simultaneously
- The pulse width is one bin, less than 200 mcs
- The moment of gamma pulse in all observational points coincide exactly with EAS
- A strong change of gamma ray background was observed.

Note, that the distance between observation detector points in space is about 1150m. They are distributed in height at 600m. So, the strong pulse of gamma emission covered quite a large area. One can see also from the Fig.5.7 that the observed energy distribution of gamma quanta has a classical RB form: small change between 40 keV (1st thr.) and 60 KeV (2st thr) and strong diminishing to 120 KeV (3st thr).

Of special interest is the sharp change of the gamma background, seen at the scan in Fig.5.7. One can see that the background value at the point 6 for three times diminishes at the trigger moment exactly. At the point 7 the background is growing up during 50 mcs before the trigger moment. Then it falls down approximately for three times. The growth of the gamma breakdown produced by cosmic rays is a consequence of the increasing of the electron flux in the thunderstorm electric field due to RB process. The sharp fall of the background means that the electric field of the thundercloud crossed by EAS has sharply diminished. In other words, an electric discharge of the cloud took place. A combined action of EAS and RB gave a macroscopic effect. So, this is just the observation of RB-EAS discharge.

Event 8.08.07

The main phase of a storm 8.08.07 with frequent lightning discharges lasted from 11:53 to 12:52. The event under discussion was registered at 12:13:35. The shower was fixed by four detectors of the EAS trigger system what means that the energy of cosmic ray particle was about 10^{15} eV. The pulse of gamma radiation was measured by detectors at the observational points 5, 6 and 7.

The scans are shown in the Fig.5.8. The strong gamma pulse simultaneous with EAS trigger at all observational points is seen. The measured radio signal is also shown in the Fig.5.8. One can see a very strong pulse of radio emission at the EAS trigger moment exactly. It means that the interaction of EAS with the cloud was accompanied by the electric discharge.

Discussion

The probability of RB-EAS event observation is determined by two factors:

- The trajectory of cosmic ray particle which generate RB-EAS event should cross the thundercloud at the distance 400-500 m from gamma detectors. Otherwise gamma mission cannot be observed due to the absorption in the atmosphere. On the other hand the same trajectory should come to our EAS trigger system to be fixed as a shower. These conditions limit the quantity of the possible trajectories.
- The second condition is natural: the value of electric field in a thundercloud crossed by EAS should be higher than the RB critical field.

This condition is evidently more often fulfilled during the main phase of the storm.

Due to these two factors RB-EAS is a rare event. It is of the order of 1% from all EAS events, observed during the thunderstorm. This estimate agrees with the results of our measurements: 4 RB-EAS events among 600 EAS. Thus the simultaneous observation of EAS with a strong gamma emission pulse in a wide space region and probability considerations demonstrates the experimental verification of the RB-EAS phenomenon, predicted for a thunderstorm atmosphere.

Note, that in a fine weather conditions analogous strong bursts of gamma emission with EAS were never registered.

The presented features of short-term flares allow to state that they arise during the development of an electron cascade in a thundercloud electric field with the subsequent slowdown of accelerated electrons in an atmosphere, i.e. they are the direct experimental confirmation of the realization of the RB- effect.

Theory

Note on theory of runaway breakdown (RB) effect

Asymptotic solution

The problem of matter breakdown is formulated in the kinetic theory in the following form. The kinetic equation for electrons is considered in the coordinate and momentum space (***r***, ***p)***. The electric field *E*, the neutral molecular density *N*, their charge *Z* and other substance parameters determining the electron collisions are considered as constants in the simplest problem statement. Collision integral is linearized. Then asymptotic over time *t* solution for the distribution function $f(\mathbf{p},t)$ of the kinetic equation has the exponential form:

$$f(\mathbf{p},t) \to f_{01}(p)\exp(\nu_1 t) + f_{02}(p)\exp(\nu_2 t).$$

It is uniform and does not depend on space coordinates. Here ν_i – eigenvalue of the linear kinetic equation, i=1,2, $f_{0i}(\mathbf{p})$ represents the corresponding eigensolution.

The exponential growth of the distribution function and consequently the growth of the electron number just mean the breakdown of the substance. Parameter ν_i determines the ionization frequency and $\nu_i^{-1} \approx \tau_i$ – the characteristic time of breakdown. The existence of two independent solutions of the linear kinetic equation means that there are two types of breakdown in any dielectric: the conventional breakdown (ν_1) and RB (ν_1).

Similarity relations

The runaway breakdown can take place in any substance. The interaction of fast electrons is coulomb and consequently it always has a similar character. Thus RB has the same structure for all substances and possesses the remarkable similarity properties. Namely, the critical field E_c is proportional to the mass density ρ in all substances. If ρ is expressed in grams per cm^3, then

$$E_c = 1{,}8\rho\left[MeV\ \mathrm{cm}^{-1}\right].$$

Correspondingly, the critical energy of runaway ε is connected with the value of the electric field *E* by the relation

$$\varepsilon \cong \frac{m_e c^2}{2\delta},$$

where $\delta = E/E_c$.

The characteristic length of breakdown *l* strongly decreases with the growth of the electric field $(\sim \delta^{-2})$, while the ionization frequency correspondingly increases:

$$\tau_2 \cong 10^{-10}\rho^{-1}\delta^{-3/2}[c],$$

$$\tau_2 \cong 10^{10}\rho\delta^{3/2}\left[c^{-1}\right].$$

In dense substances with $\rho \approx 10-100$ g cm^{-3} the characteristic times of the breakdown are extremely small. It should be added that these times rapidly fall down with the growth of the parameter δ.

Note, that the indicated similarity relations are correct in the limited range of variation of the parameter δ:

$$1{,}5 \le \delta \le 100-150.$$

Runaway breakdown in atmosphere

The dependence of RB ionization frequency ν_2 for air on the electric field value E is presented in Fig.5.3. One can see that RB ionization frequency monotonically increases with the field E ($\sim E^{3/2}$). At the same time the conventional breakdown ionization frequency ν_1 at first increases very rapidly with the increasing of E (approximately as $\sim E^{5,5}$), but then saturates (see [1-3]).

It is important that RB can take place even at low values of electric field, i.e. in the *small field*, when the condition $E_{th} > E > E_c$ is fulfilled. In the case the ionization frequency is extremely high: $\nu_2 > 10^7 - 10^8$ c^{-1}.

The conventional breakdown can not take place in the small field, it occurs at $E > E_{th}$. Moreover, although the ionization frequency of the conventional breakdown very rapidly increases with the increasing E it still remains less than the RB ionization frequency up to the value $E \cong 2E_{th}$. This circumstance can be highly important and can lead to the occurrence of the high number of fast electrons in the conventional discharge at $2E_{th} \geq E \geq E_{th}$. It may be assumed that it is the cause of the observed bursts of gamma ray emission both in a lightning leader [4-6] and in discharges studied in laboratories [7-9].

So, RB is the main breakdown in air relative to the quickness of ionization increasing not only at $E < E_{th}$ but at larger values of electric field up to $E = 2E_{th}$.

The second important parameter presented in Fig.5.9 is the characteristic length l. It determines the minimal space scale of the breakdown range. One can see that in small fields the length is very large ($l \approx 30 - 50$ m). But it rapidly decreases with the increasing of electric field E ($\sim E^{-2}$), so that even for $E \approx (1-2)E_{th}$ the length l becomes of the order of 10-30 cm. At high field values $E >> E_{th}$ the characteristic length l becomes rather small. It demonstrates that while at small electric fields the investigation of RB is possible only in thunderclouds, the investigation at higher electric fields is possible on laboratory installations as well.

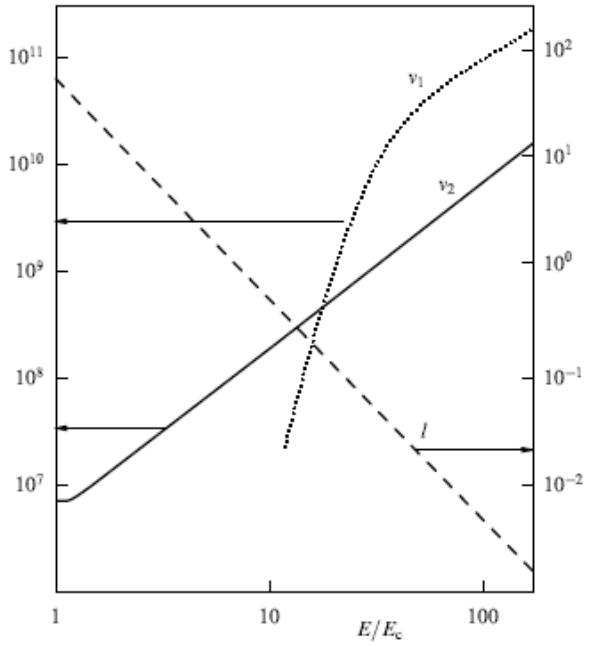

Fig.5.9. Dependence of the conventional breakdown ionization frequency ν_1 and of the RB ionization frequency ν_2 on the electric field value (left scale, c^{-1}).

Dependence of the avalanche growth length *l* on the electric field value (right scale, m) is presented as well.

Effect of cosmic rays

To RB occur besides the fulfillment of the condition $E > E_c$ the presence of fast seed electrons having energy exceeding the runaway energy ($\varepsilon > \varepsilon_c$) is needed. These conditions are realized in thunderclouds. Observations show that maximal electric fields in thunderclouds are close to the critical RB field E_c [1,2,9]. The secondary electrons of cosmic rays (CR) serve as fast seed particles. Their mean flux density at heights 4-8 km is relatively high: $\Phi_e \approx 10^3$.

The essential difference of RB from conventional breakdown consists in the effective generation of X and gamma emission. Exactly the observation of gamma emission with $\varepsilon \approx 50-100$ keV indicates the possible RB realization. Simultaneously strong lectric currents could be excited, leading to the generation of radio emission.

It is natural that the number of runaway electrons is proportional to the number of seed ones generated in the interaction of CR with the air. The total seed electron number N_e in an EAS increases proportional to the energy of the primary CR particle. For example, N_e is about 10^6 in the shower generated by the primary CR particle with the energy $E_{CR} \approx 10^{18}$ eV. If $E_{CR} \approx 10^{18}$ eV, then $N_e \approx 10^{10}$.

While an EAS passes through the thundercloud where $E > E_c$ the runaway electrons avalanche grows up and the number of energetic electrons in the EAS increases exponentially. Simultaneously the number of thermal electrons increases for several millions times. All together they generate the RB-EAS discharge [10]. Naturally, this discharge should be accompanied by the strong pulse of gamma emission due to the large number of fast electrons.

References

- Borisov N.D., Gurevich A.V., Milikh G.M., “Artificial ionized layer in atmosphere” (Moscow. IZMIRAN, 1986, in Russian)
- Papadopoulos K et al., J. Geophys. Res. **98** (A10) 17593 (1993)
- Gurevich A.V., Borisov N.D., Milikh G.M. “Physics of microwave discharges” (Amsterdam Gordon and Breach, 1997)
- Moore et al. Geophys. Res. Lett. **28** 2141 (2001)
- Dwyer J.R. et al., Geophys. Res. Lett. **32** L01893 (2005)
- Howard J. et al., Geophys. Res. Lett. **35** L13817 (2008)
- Dwyer J.R. et al., Geophys. Res. Lett. **32** L20809 (2005)
- Rahman M. et al., Geophys. Res. Lett. **35** L06805 (2008)
- Nguyen C.V., van Deursen A.P.J., Ebert U.J., J. Phys D **41** 234012 (2008)
- Gurevich A.V., Zybin K.P., Roussel-Dupre R.A., Phys. Lett A **254** 79 (1999)

ATTACHEMENT

List of published papers

1. A.V. Gurevich, K.P. Zybin, Strong field aligned scattering of UHF radio waves in ionospheric modification, Phys. Lett. A **358** (2006)159 – 165.
2. A.V. Gurevich, K.P. Zybin, Yu.V. Medvedev, “Runaway breakdown in strong electric field as a source of terrestrial gamma flashes and gamma bursts in lightning leader steps”, Phys. Lett. A **361** (2007) 119 – 125.
3. Antonova V.P., L.I. Vildanova, A.V. Gurevich, K.P. Zybin, A.N. Karashtin, S.V. Kryukov, M.O. Ptitsyn, A.P. Chubenko, Yu.V. Shlyugaev, A.L. Shepetov, Study of Interrelation between Processes in the Thunderstorm Atmosphere and Energetic Cosmic Rays with the Groza Tien Shan Developmental Installation, Technical Physics, 2007, Vol. 52, No. 11, pp. 1496–1501.
4. Gurevich A.V. "Nonlinear effects in the ionosphere" *Phys. Usp.* **50** (2007) 1091-1122 .
5. A.V. Gurevich, A.N. Karashtin, V.A. Ryabov, A.P. Chubenko, A.L. Shepetov, Nonlinear phenomena in the ionospheric plasma. Effects of cosmic rays and runaway breakdown on thunderstorm discharges, Physics-Uspekhi 52 (2009) 735 745.
6. G. Milikh, A. Gurevich, K. Zybin, J, Secan "Perturbations of GPS signals by the ionospheric irregularities generated due to HF-heating at triple of electron gyrofrequency" Geophys. Res. Lett., VOL. 35, L22102, doi:10.1029/2008GL035527, 2008.
7. A.P. Chubenko, A.N. Karashtin, V.A. Ryabov, A.L. Shepetov, V.P. Antonova, S.V. Kryukov, G.G. Mitko, A.S. Naumov, L.V. Pavljuchenko, M.O. Ptitsyn, S.Ya. Shalamova, Yu.V. Shlyugaev, L.I. Vildanova , K.P. Zybin, A.V. Gurevich, “Energy spectrum of lightning gamma emission”, Physics Letters A 373 (2009) 2953–2958.
8. A.V. Gurevich, G.G. Mitko, V.P. Antonova, A.P. Chubenko, A.N. Karashtin, S.V. Kryukov, A.S. Naumov, L.V. Pavljuchenko, M.O. Ptitsyn, V.A. Ryabov, S.Ya. Shalamova, A.L. Shepetov, Yu.V. Shlyugaev, L.I. Vildanova, K.P. Zybin, “An intracloud discharge caused by extensive atmospheric shower”, Physics Letters A 373 (2009) 3550–3553.
9. V.P. Antonova, L.I. Vildanova, A.V.Gurevich, K.P. Zybin, A.N. Karashtin, S.V.Kryukov, V.A. Ryabov, M.O. Ptitsyn, A.P. Chubenko, Yu.V.Shlyugaev, A.L.Schepetov , «Influence of cosmic rays and the runaway-electron breakdowns on thunderstorm processes in the atmosphere», Radiophysics and Quantum Electronics, V.52 #9 (2009) 627.
10. K.V. Bochkarev, K.P. Zybin “Ultra low frequency pulsation generation under the action of modulated microwave power on ionosphere”, Physics Letters A 374 (2010) 1508–1513.

List of presentations at conferences

Invited talks, VII International Suzdal URSI SymposiumМеждународном on Ionosphere Modification ISS-2007, Troitsk, October 16 – 18, 2007:

1. A.V. Gurevich “Runaway breakdown and problem of lightning”.
2. K.P. Zybin "Runaway breakdown in strong electric field".
3. V.P. Antonova, L.I. Vildanova, A.V. Gurevich, K.P. Zybin, A.N. Karashtin, S.V. Kryukov, V.A. Ryabov, V.V. Piskal, M.O. Ptitsyn, A.P. Chubenko, Yu.V. Shlyugaev and A.S. Shepetov, "Study of the combined effects of runaway breakdown and cosmic rays on lightning processes in thunderstorm atmosphere".

A.N. Karashtin, Yu.V. Shlyugaev and A.V. Gurevich, "Experimental investigation of close thunderstorm lightning discharge. Radio emission in a wide frequency range".